Powerline Bushfire Safety Program: Research and Development Round II

Performance Analysis of Compensated Distribution Networks in Bushfire Prone Areas

THE STATE OF VICTORIA

as represented by its

DEPARTMENT OF ENVIRONMENT, LAND WATER AND PLANNING

AND

DEAKIN UNIVERSITY

Table of Contents

Executive Summary

The severity of Australian bushfires in almost every summer has been impacting every aspect of life. The Victorian Government proactively acted to reduce the impacts of bushfires through the implementation of recommendations provided by the 2009 Victorian Bushfire Royal Commission (VBRC). As indicated in the VBRC's report powerlines faults were responsible for some major bushfires in 2009, and the Victorian Government has taken a world-leading initiative to utilise an advanced protection technology called, rapid earth fault current limiters (REFCLs) for 45 zone substations in bushfire-prone areas to minimise the risks of powerline bushfires. However, distribution network owners face several challenges for adopting REFCLs, which include the identification of fault locations, characteristics of cross-country faults, network damping and network imbalances. This project is aimed to provide research input to some of the challenges faced by distribution system operators commissioning REFCL technology in 22kV substations.

The first technical contribution of this project is to develop an algorithm to locate fault and to estimate the voltage at fault location. To minimise bushfire risk arising from powerline bushfire, it is very important to estimate the faulty phase voltage at the fault location for risk assessment and subsequent actions. Currently, the arc suppression devices used in bushfire-prone areas have very limited capability in this regard. Therefore, an algorithm needs to be developed to estimate the voltage at the fault location using the available information at the distribution substation.

The second technical contribution is to analyse the sensitivity of parameters that affect voltages at the fault locations. The effect of several parameters including inductance of the inductor coil which is connected between the neutral point of substation transformer and ground, fault resistance, properties of cables (line capacitance, resistance, and inductance), location of fault, loads at the faulty feeder (both magnitude and power factor), fault inception angle, and structures of the network on fault voltage and current have been investigated.

This report also analyses the impact of network reconfiguration on damping and provides a robust estimation of damping in the REFCL-compensated power distribution network. Damping represents resistive leakage current (to ground) of the network. It can be leakages through any asset connected to the ground, such as pole mount transformers, surge arresters, insulators, poles, etc. It also depends on series resistance of the conductor/cable. For effective operation of the REFCL devices, damping needs to be estimated with a great degree of accuracy.

Furthermore, a mathematical model is presented that can identify the impact of mutual coupling on network imbalance. The model identifies influencing parameters by providing a thorough analysis of the coupling effect of 22kV distribution and 66kV sub-transmission lines.

Chapter 1

Introduction

The overarching objective of the project named "**Performance Analysis of Compensated Distribution Networks in Bushfire Prone Areas**" is to provide a performance assessment to investigate the potential impacts of implementing Rapid Earth Fault Limiter (REFCL) technology on selected AusNet Services rural networks.

The REFCL instantly detects single line-to-ground faults and minimises the fault current, as well as reduces the phase voltage for the faulty feeder. At this instant, the voltages of other two phases increase, and these lines continue to supply power during the faulted condition. This is not an issue for a temporary fault but challenging for permanent faults for which there could be several options: (a) identifying the fault location under condition of full neutral voltage displacement; (b) detecting fault in a traditional way by activating existing relays; and (c) tripping the whole feeder. The first option is a feasible one, but it requires the development of a new approach, while the second option still has the risk of causing bushfires, and the last option will affect the reliability. However, the identification of only the fault location will not resolve these issues, as it is also important to analyse the behaviours of the faulty phase voltage including the factors affecting this voltage so that preventive actions can be taken.

The network damping is considered another important challenge for the operation of REFCLs. The leakage current depends on weather conditions, which in turn affects the neutral voltage and hence, the fault detection capability of REFCLs is adversely affected, as a constant threshold is used for the neutral voltage rather than an adaptive one based on the real-time calculation of the network damping. The network imbalance also severely affects the fault detection sensitivity of REFCLs. To address these issues, this project has some specific tasks, objectives, and deliverables which are discussed in the following sections.

1.1 Tasks

The project has four tasks which are outlined as follows:

(i) *Task 1 - Identification of fault location and estimation of the voltage at fault location*:

The arc suppression devices can detect faults and reduce fault current, as well as the phase-to-ground voltage of the faulty phase. However, it is extremely important to estimate the phase voltage of the faulty phase at the fault location, as a reduction of the faulty phase voltage assists to minimise bushfire risk. Currently, the arc suppression devices used in bushfire-prone areas have very limited capability in this regard. Therefore, an algorithm needs to be developed to estimate the voltage at the fault location using the available information at the distribution substation. Since the estimation of the voltage at the fault location requires the identification of the location of the phase-to-ground fault in the compensated network, the main feature of the algorithm is the identification of the fault location. Furthermore, the proposed approach compares phase voltages of healthy phases to make the final decision regarding the estimation of the fault location and phase-to-ground voltage at the fault location. In this way, the proposed estimation algorithm assists distribution network service providers to make effective decisions and to maintain the thermal energy within 0.1 A^2s so that bushfire risk is reduced. Furthermore, it assists providers to reduce the duration of voltage collapses during faults.

(ii) *Task 2 - Sensitivity analysis of different factors affecting the voltage at fault location*:

To develop an appropriate mechanism to reduce the voltage at fault location and to maintain the thermal energy within the limit, it is essential to investigate the impacts of different factors that affect the voltage at the fault location. There are several factors within the system that affect the voltage at the fault locations, which include, the value of inductance of the arc suppression coil, loads in the faulty feeder (both magnitude and power factor), location of the feeder, properties of cables, and structures of the network (especially, purely radial, or radial with many branches, as in AusNet Services' distribution networks in bushfire-prone areas). The sensitivity of all these factors on the voltage at the fault location is analysed. A ranking of the different factors is then produced highlighting the severity or contribution of each parameter. This assists the distribution network service providers to concentrate on factors that severely affect the phase voltage at the fault location and to take appropriate steps to mitigate the adverse effects of powerline bushfires.

(iii) *Task 3 - Development of an adaptive approach for calculating the network damping based on real-time measurement:*

The network damping severely affects the fault detection sensitivity of arc suppression devices as the higher values of the network damping decrease the neutral voltage. Therefore, it is important to maintain the network damping within a reasonable range, preferably to a low value. Hence, the objective of this task is to develop an adaptive prediction mechanism to predict the severity of the leakage resistance on the overall network damping based on the network parameters. Additionally, another aim of this part is to analyse REFCL compensated distribution network models to identify sensitive parameters that aid in developing a damping limiting strategy.

(iv) *Task 4 - Analysing the impacts of sub-transmission lines on the network imbalance of distribution lines due to sharing the same pole:*

It has been investigated that 66 kV lines have significant impacts on the unbalance current at 22 kV feeders if they share the same pole (or run in parallel to each other with minimal distance). Especially, the change in the unbalance current is observed, while switching the 66 kV line. On the other hand, REFCL devices are sensitive to unbalance current for detecting faults in the network. Therefore, the objective of this task is to develop a mathematical model required to investigate the actual relationship between the unbalance current at the 22 kV feeder and the 66 kV line parameters.

1.2 Objectives

The project has some specific objectives which are to:

(i) Develop an algorithm for identifying fault location and estimate the voltage at fault location.
(ii) Analyse the sensitivity of different factors affecting the voltage at the fault location.
(iii) Develop an adaptive approach for calculating the network damping based on the real-time measurement.
(iv) Analyse the impacts of the sub-transmission lines on the network imbalance of distribution lines due to sharing the same poles.

1.3 Deliverables

The project has some specific deliverables related to the above-mentioned tasks. The deliverables are as follows:

(i) *An algorithm for estimating the fault location and the voltage at the fault location*.

In this analysis, an impedance-based fault location method is used to identify the fault location and estimate the voltage at fault location. One of the benefits of this method is that the measured data available at substation can be used to implement the method.

(ii) A ranking of different factors affecting the voltage at the fault location.

There are many factors that affect the voltage at fault location that are mentioned in the Task-2 of Section 1.1. Each possible factor that may affect the voltage at fault location is analysed in this task. Based on their effects, a ranking of them is produced.

(iii) An adaptive scheme for calculating the network damping using real-time information.

The damping of the distribution feeder is estimated in this task from measurements at different points of the REFCL protected power distribution network.

(iv) A framework for analysing the impacts of sub-transmission lines on the network imbalance of distribution lines.

The actual relationship between the unbalance current at the 22 kV feeder and the 66 kV line parameters is investigated. Moreover, a suitable strategy has been devised to effectively analyse the impacts of 66 kV lines on the unbalance of 22 kV lines.

The mechanism, operations, and processes employed to complete the above-mentioned tasks have been presented in detail in this document. There is no confidential information in this report. Therefore, this final report is a stand-alone document.

1.4 Brief outline of the report

Chapter 1 provides an overview of the project tasks, objectives, and deliverables. Chapters 2 to 4 provide the research outcomes on the four tasks as part of this project.

Chapter 2 deals with locating fault and estimating voltage at fault location. To minimise risk of ignition arising from powerline bushfire, it is particularly important to estimate the faulty phase voltage at the fault location. Currently, the arc suppression devices used in bushfire-prone areas have limited capability in this regard. Therefore, an algorithm needs to be developed to estimate the voltage at the fault location using the available information at the distribution substation which is also discussed in Chapter 2.

Chapter 3 deals with identification of parameters that affect voltage at the fault locations. The effect of several parameters including inductance of the inductor coil which is connected between neutral point of substation transformer and ground, fault resistance, properties of cables (line capacitance, resistance, and inductance), location of fault, loads in the faulty feeder (both magnitude and power factor), fault inception angle, and structures of the network on fault voltage and current have been investigated in Chapter 3.

Chapter 4 analyses the impact of network reconfiguration on damping and provides a robust estimation of damping in the REFCL compensated power distribution network. Damping represents resistive leakage current (to ground) of the network. It can be leakages through any asset connected to the ground, such as pole mount transformers, surge arresters, insulators, even poles, etc. It also depends on series resistance of the conductor/cable. For effective operation of the REFCL devices damping needs to be estimated with a great degree of accuracy, which Chapter 4 deals with.

Chapter 5 presents a mathematical model to identify the impact of mutual coupling on network imbalance. The model identifies influencing parameters by providing a thorough analysis of the coupling effect of 22kV distribution and 66kV sub-transmission lines.

Chapter 6 provides future outlooks of the research and conclusion.

Chapter 2

Identification of Fault Location and Estimation of the Voltage at Fault Location

2.1 Introduction

This chapter covers the first task of the project which is “Identification of the fault location and estimation of the voltage at fault location”. In this analysis, an impedance-based fault location method is used to identify the fault location and estimate the voltage at fault location due to its low implementation cost**.** In addition, the required data for the implementation of the method can easily be obtained from the substation measurement system**.** Since the fault current in the compensated network is much lower than traditional solidly ground network, the implementation of the impedance-based fault location faces extra challenges. In the next successive sections, the algorithm related to the identification of fault location and estimation of the voltage at fault location of a compensated distribution network is presented.

2.2 Intended outcome

An algorithm needs to be developed to estimate the voltage at the fault location using the available information at the distribution substation. One of the important features of this algorithm will be the identification of the fault location.

2.3 Background

Electric power transmission and distribution systems are often subjected to the electric power failure due to the various reasons such as electrical equipment failure, conducting with trees and so on. The interruption in the electric supply reduces the reliability of the system. It is extremely important to estimate the phase voltage of the faulty phase at the fault location, as a reduction of the faulty phase voltage assists to minimise bushfire risk. Therefore, the identification of fault location is very important to reduce the duration of power outage and identify the voltage at fault location. Due to the inhomogeneity of distribution line, huge number of branches and load uncertainty, the ways of fault location for distribution lines face more challenges than those for transmission lines [1].

Three types of methods for identification of fault location in distribution system are generally utilised such as impedance-based methods, travelling wave-based methods and knowledge-based methods [1]-[4]. As the distribution line is inhomogeneous, additional reflected waves are generated at discontinuous points along with the wave generated at fault point. The one of the challenges of the implementation of the travelling wave-based fault location method is to differentiate the actual reflected wave from the waves generated at other points [2]. In the knowledge-based method, various machine learning methods such as artificial neural network and fuzzy-c mean clustering are used to identify the fault locations [5], [6]. These methods generally depend on a large amount of input data which is often unavailable [2].

On the other hand, the impedance-based method [1], [7], [8] for identification of fault location gets high research attention due to its low implementation cost. In addition, only measured voltage, and current data at substation along with line parameters (resistance, inductance, and capacitance) can be exploited to identify the fault location. In this research, impedance-based method [1] is considered to identify the fault location. There are many impedance-based fault location methods are found in the literature [1], [7], [8], which are mainly for solidly ground network. The fault current of the compensated distribution network due to single line to ground fault is much lower than that of solidly ground distribution network. Thus, the identification of fault location of a compensated network using impedance-based method is more challenge than that of the solidly ground network. In this analysis, single to ground fault is considered for identification of fault location as about 70% of faults, that are subjected to the bushfire powerline, is single line to ground fault [9].

2.4 Conventional impedance-based fault location

To implement the impedance-based fault location method, a simple solidly ground distribution network is firstly considered as shown in Fig. 2.1. A single line to ground fault is considered in a phase-line at point F as shown in Fig. 2.1 through fault resistance R_f. From Fig. 2.1, the voltage across the fault resistance can be written as follows [1]:

$$I_f R_f = E_{an} - d \times (Z_{aa} I_a + Z_{ab} I_b + Z_{ac} I_c) \tag{2.1}$$

where Z_{aa} is line self-impedance, Z_{ab} and Z_{ac} are mutual impedance, I_a and I_b and I_c are line or phase currents, E_{an} is the voltage at sending end with respect to neutral, d ($0 < d \leq 1$) is the fault distance, and R_f is fault resistance.

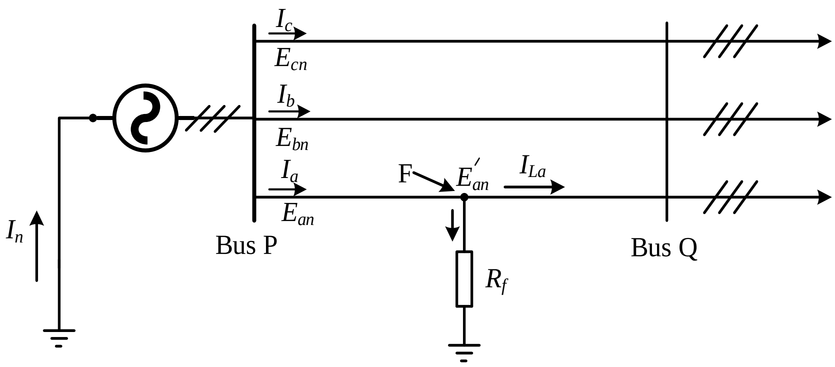

Fig. 2.1. A simple solidly ground distribution network.

By separating imaginary and real parts of the (2.1), one can write as [1],

$$d = \frac{E_{anr} I_{fi} - E_{ani} I_{fr}}{M\, I_{fi} - N\, I_{fr}} \tag{2.2}$$

where

$$M = (Z_{aar} I_{ar} - Z_{aai} I_{ai} + Z_{abr} I_{br} - Z_{abi} I_{bi} + Z_{acr} I_{cr} - Z_{aci} I_{ci} \tag{2.3}$$

$$N = (Z_{aar} I_{ai} + Z_{aai} I_{ar} + Z_{abr} I_{bi} + Z_{abi} I_{br} + Z_{acr} I_{ci} + Z_{aci} I_{cr}. \tag{2.4}$$

Here, subscripts r and j indicate the real and imaginary parts of the corresponding phasors. To identify the fault distance of a solidly ground network, (2.2) is mainly used in the impedance-based fault location method [1].

In the same way, a simple compensated distribution network as shown in Fig. 2.2 is considered in this analysis, where a variable inductor is connected between ground and neutral point of the substation transformer. If a single line to ground fault is considered at the same point F as mentioned for solidly ground network through fault resistance R_f, the voltage across the fault resistance for compensated network can be written as follows:

$$I_f R_f = E_{an} - V_n - d \times (Z_{aa} I_a + Z_{ab} I_b + Z_{ac} I_c) \tag{2.5}$$

where V_n is the voltage across the inductor.

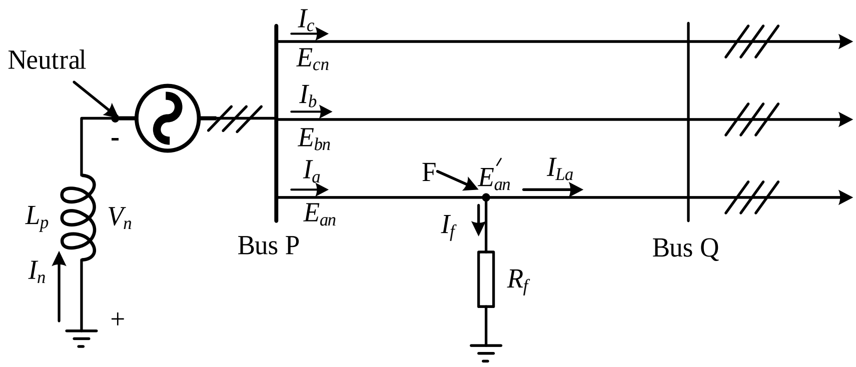

Fig. 2.2. A simple compensated distribution network.

For solidly ground network as shown in Fig. 2.1, the V_n is zero, and thus the phase voltage totally drops across the fault resistance and the corresponding current in the faulty phase becomes high as shown in Fig. 2.3. On the other hand, it is observed from (2.5) and Fig. 2.2, that in the case of compensated distribution network, a significant voltage drop occurs across the inductor that is connected in series with fault resistance. Consequently, the change in current of the faulty phase is quite low, and the voltage across the fault resistance also becomes drastically low. Fig. 2.4 shows the prefault and after fault phase currents for a typical compensated distribution network. It is observed from Fig. 2.4 that after occurring fault, the current in faulty phase changes slightly.

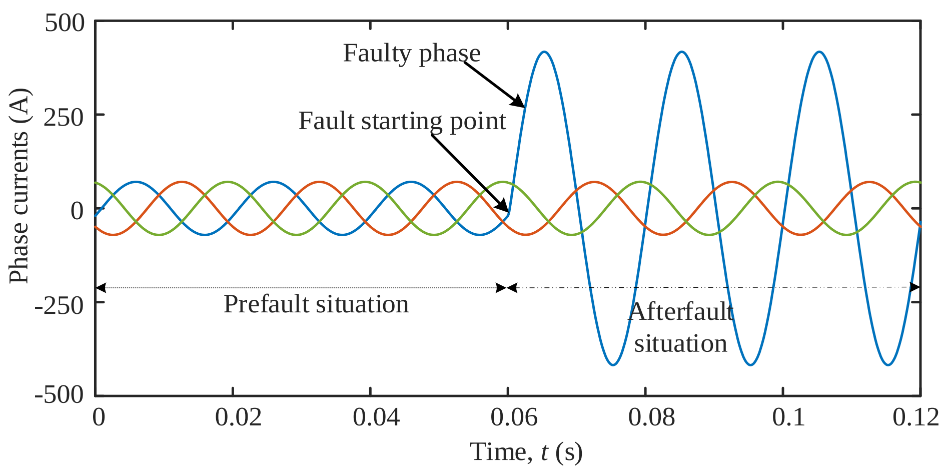

Fig. 2.3 Phase currents of a typical solidly ground distribution network after occurring single line to ground fault.

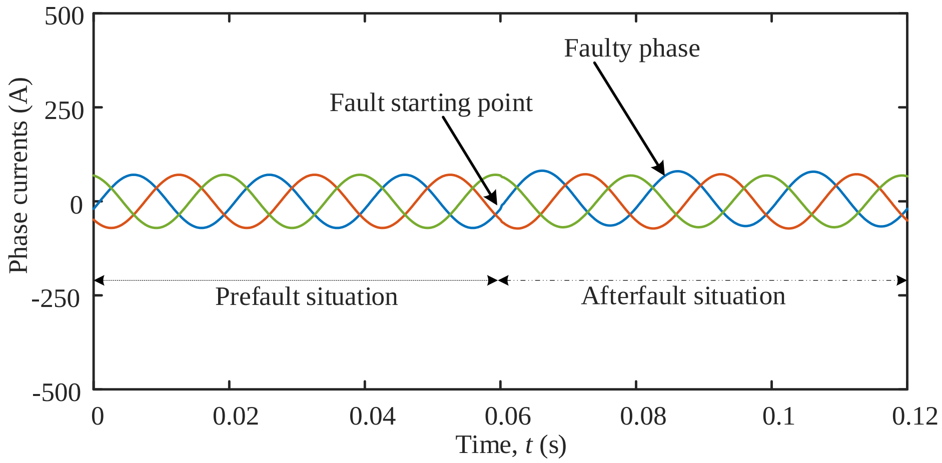

Fig. 2.4 Phase currents of a typical compensated distribution network after occurring single line to ground fault.

By separating imaginary and real parts of the (2.5) for a compensated distribution network as the same as solidly ground distribution network, one can write as,

$$d = \frac{E_{anr}I_{fi} - E_{ani}I_{fr} - V_{nr}I_{fi} + V_{ni}I_{fr}}{M\,I_{fi} - N\,I_{fr}} \tag{2.6}$$

where M and N are calculated by (2.3) and (2.4), respectively.

Using Kirchhoff's current law at the fault point as shown in Fig. 2.2, the fault current can be expressed by

$$I_f = I_a - I_{La} \tag{2.7}$$

where I_{La} is the downstream current following toward the next bus after fault. The process of the calculation of I_{La} is given in Section 2.4.3. The above-mentioned equations (2.3) - (2.7) along with line parameters, and the measured data of E_{an}, E_{bn}, E_{cn}, V_n, I_a, I_b and I_c at substation can be used to identify the fault location. Therefore, before implementation of the fault identification technique, it is necessary to be modelled the line section where the line parameters are associated. Line branches also need to be modelled as the distribution line generally consists of many branches. In addition, the modelling of loads which are usually connected with different buses of the network are necessary to be considered. In the following subsections, the modelling of distribution line, modelling of load and modelling of branch are explained in detail.

2.4.1 Distribution line model

The electrical line is generally considered as a combination of resistance, inductance and capacitance which are modelled as either distributed or lumped parameters depending on the length of line. As distribution line is generally short or medium length, lumped parameters can be used to model the line as shown in Fig. 2.5. Moreover, after occurring the earth fault, the system becomes unbalanced, and the unbalanced network is then generally analysed as a combination of sequence values of positive, negative and zero sequences resistances, inductances, and capacitances. It is worth mentioning that positive and negative sequence values of the line parameters are generally considered as equal values.

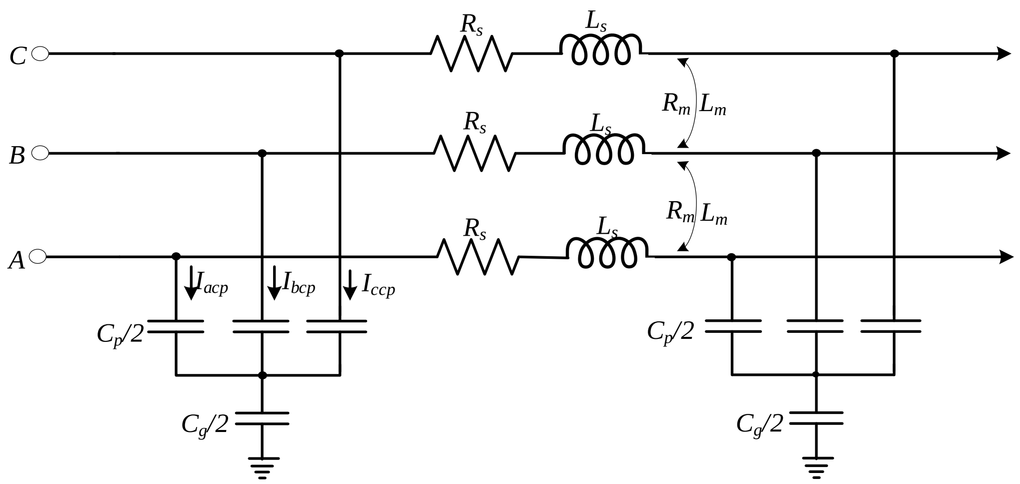

Fig. 2.5 Modelling of a distribution line section [2.10].

In this analysis, the self-impedances of each phase are considered as equal that is given by [10]

$$Z_{aa} = Z_{bb} = Z_{cc} = R_s + j\omega L_s \tag{2.8}$$

with

$$R_s = \frac{(2R_1 + R_0)}{3} \tag{2.9}$$

and

$$L_s = \frac{(2L_1 + L_0)}{3} \tag{2.10}$$

where Z_{aa}, Z_{bb} and Z_{cc} are self-impedances of phases A, B and C respectively, and R_1 and R_0 are the positive and zero sequence resistances of the section line, and L_1 and L_0 are the positive and zero sequence inductances of the section line, respectively.

In the same way, one can obtain the mutual impedances from [10], which are as follows:

$$Z_{ab} = Z_{bc} = Z_{ac} = R_m + j\omega L_m \tag{2.11}$$

with

$$R_s = \frac{(R_0 - R_1)}{3} \tag{2.12}$$

and

$$L_s = \frac{(L_0 - L_1)}{3} \tag{2.13}$$

where Z_{ab}, Z_{bc} and Z_{ac} are the mutual impedances of the line section which are considered as equal in this analysis.

The C_p and C_g as mentioned in Fig. 2.5 can be calculated as follows:

$$C_p = C_1 \tag{2.14}$$

$$C_g = 3C_1C_0/(C_1 - C_0) \tag{2.15}$$

where C_1 and C_0 are positive and zero sequence capacitances of the line section, respectively.

The line resistance and inductance are already considered in the equations of the impedance-based fault location method as shown in (2.3) - (2.6). Therefore, it is necessary to consider the line capacitance in the identification of fault location method.

As the phase voltages with respect to ground becomes unbalanced after occurring the earth fault, considerable current flow through the C_g in the distribution line model. To calculate the currents passing through the resistance and inductance, the current passing through the capacitance needs to be subtracted from the input current. Therefore, it is necessary to be calculated the current passing through the capacitance for each phase. To obtain the generalised current passing through each phase capacitance, line capacitances are concentrated in one side as shown in Fig. 2.6. After applying Kirchhoff's voltage law in each phase, the following equations can be written,

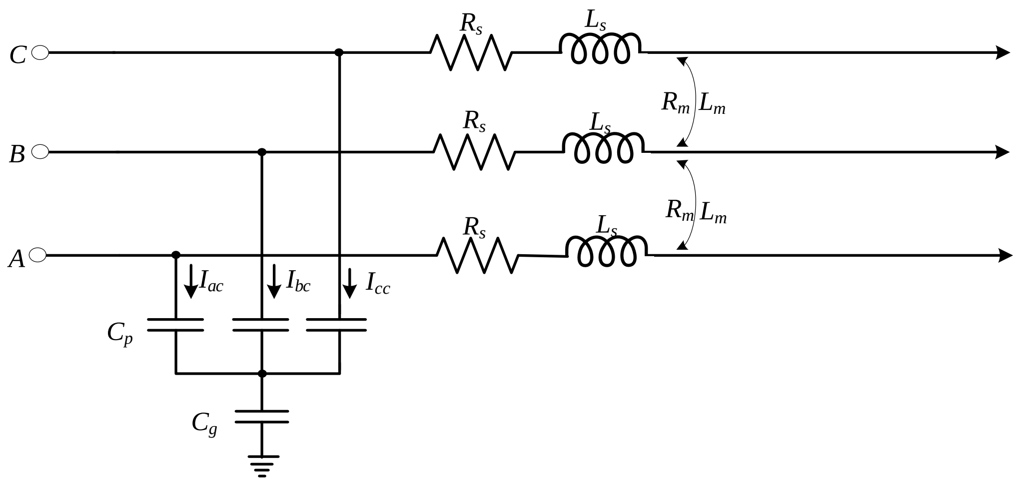

Fig. 2.6 Distribution line model with capacitance concentrated at beginning of the line section.

$$I_{ac} = -\frac{E_{an} - V_n + jX_{cg}I_{bc} + jX_{cg}I_{cc}}{j(X_{cg} + X_{cp})} \tag{2.16}$$

$$I_{bc} = -\frac{E_{bn} - V_n + jX_{cg}I_{cc} + jX_{cg}I_{ac}}{j(X_{cg} + X_{cp})} \tag{2.17}$$

$$I_{cc} = -\frac{E_{cn} - V_n + jX_{cg}I_{ac} + jX_{cg}I_{bc}}{j(X_{cg} + X_{cp})} \tag{2.18}$$

where $X_{cp} = 1/(2\pi f C_p)$ and $X_{cg} = 1/(2\pi f C_g)$, and I_{ac}, I_{bc} and I_{cc} are the capacitive currents of the corresponding phases, f is the frequency, and E_{an}, E_{bn} and E_{cn} are the phase voltages with respect to neutral. By solving the above equations, the currents I_{ac}, I_{bc} and I_{cc} can be easily calculated.

2.4.2 Load model

After occurring single line to ground fault in the compensated distribution system, the magnitude of phase to neutral voltage at fault location changes slightly as the fault current is very low compared to solidly ground system. Thus, in the compensated distribution system, after occurring the single line to ground fault, the load current can be calculated as usual which is as follows:

$$I_L = E_{an}\, Y_L \tag{2.19}$$

where I_L is the load current, E_{an} is the voltage at bus where load is connected, and Y_L is the load admittance.

2.4.3 Branch model

For modelling of a branch on the identification of fault location method, a network with branches is firstly assumed as shown in Fig. 2.7, where a single line to ground fault occurs in a line section between buses 7 and 8. If current entering to the bus 7 is considered as I_7 and the voltage at bus 7 with respect to the neutral is E_{an}, the current entering to line section between buses 7 and 8 can be obtained by,

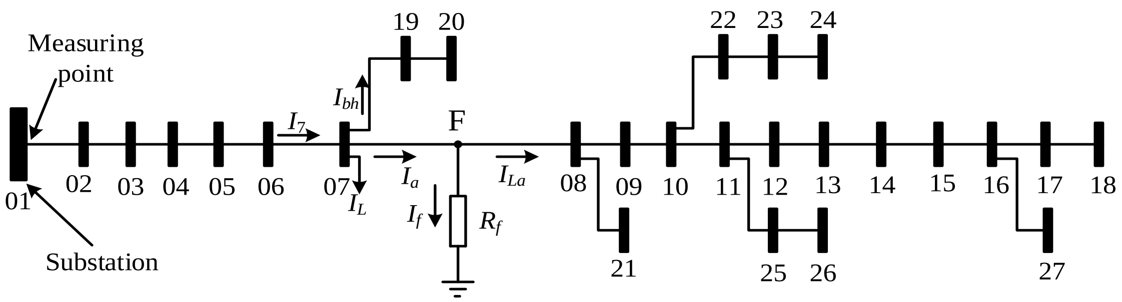

Fig. 2.7 A typical radial distribution network with branches.

$$I_a = I_7 - I_{bh} - I_L \tag{2.20}$$

where I_{bh} is the branch current which can be calculated as follows:

$$I_{bh} = E_{an} Y_{RLeqb} + I_{bhc} \tag{2.21}$$

where Y_{RLeq} is the equivalent admittance excluding the capacitance toward the branch from bus 7, and I_{bhc} is the capacitive current due to the equivalent admittance toward the branch excluding line resistance, inductance, and load impedance, i.e., considering only the line capacitance. The current I_{bhc} is calculated using (2.16) - (2.18), where $X_{cp} = 1/\left(2\pi f \sum C_{peqbh}\right)$ and $X_{cg} = 1/\left(2\pi f \sum C_{geqbh}\right)$. The $\sum C_{peqbh}$ and $\sum C_{geqbh}$ indicate the sum of C_p and C_g of line toward the branch, respectively.

In the same way, the current I_{La}, i.e., the current outgoing from fault point to the nearest bus as mentioned in (2.7) and Fig. 2.2, can be calculated by the following equation

$$I_{La} = E'_{an} Y_{RLeqLa} + I_{ceqLa} \tag{2.22}$$

where E'_{an} is the voltage with respect to neutral at fault point, Y_{RLeqLa} is the equivalent admittance excluding the line capacitance toward the downstream part of network from fault point, and I_{ceqLa} is the current due to downstream line capacitance. The current I_{bhc} is calculated using (2.16) - (2.18), where $X_{cp} = 1/\left(2\pi f \sum C_p\right)$ and $X_{cg} = 1/\left(2\pi f \sum C_g\right)$. The $\sum C_p$ and $\sum C_g$ indicate the sum of C_p and C_g of the downstream line, respectively. The voltage at the fault point with respect to neutral as mentioned in (2.22) can be written as:

$$E'_{an} = E_{an} - d(Z_{aa} I_a + Z_{ab} I_b + Z_{ac} I_c) \tag{2.23}$$

In the same way, other two phases' voltages at fault location can be calculated.

As the modellings related to the identification of fault location using impedance-based method are discussed in the above-mentioned subsections, the final algorithm of the impedance-based fault location method for compensated distribution network can be summarised as follows:

(i) Firstly, the fault is considered at a point in a line section between two buses, i.e., a random value of d ($0 < d \leq 1$) is initially considered.
(ii) Then, find the voltage at fault point with respect to neutral, E'_{an} by (2.23)
(iii) Calculate the downstream current I_{La} by (2.22).
(iv) Calculate the fault current I_f by (2.7)
(v) Fault distance d is calculated by (2.6).
(vi) If the error between two successive calculated d is within specific limit, then go to step (vii) otherwise go to step (ii).
(vii) Check line section which is not considered for identifying fault location. If available, go to step (i) for a new line section, otherwise go to step (viii)
(viii) Find out the line sections where the corresponding values of d within $0 < d \leq 1$.
(ix) Stop.

2.5 Proposed modified impedance-based fault location method

Before starting the proposed modified impedance-based fault location method, it needs to be found out the limitation of the above-mentioned conventional (existing) impedance-based fault location method. Therefore, the conventional impedance-based fault location method is firstly implemented in the section. To implement the above-mentioned fault identification method as discussed in Section 2.4, a part of an AusNet's compensated distribution network is considered in this chapter. The corresponding line parameters (Resistance, inductance, and capacitance) of the network are also exploited in the analysis. It is advantageous to mention the bus number in the implementation of fault location method so that line section can easily identified. Fig. 2.8 shows the considered distribution network with numbered buses. In this analysis, MATLAB Simulink platform is firstly used to analyse the network. After obtaining the required fault data, MATLAB program/code is used to implement the fault location method.

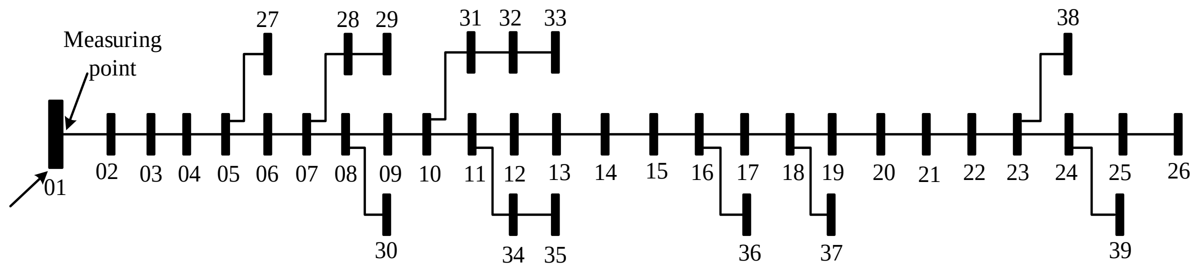

Fig. 2.8 The considered network with bus numbers.

Bus 1 in Fig. 2.8 is selected as a sub-station where there is a provision of measurement voltages and currents of the compensated network. After that single line to ground fault is separately done at different sections of the network at different fault resistance, and their corresponding sending end phase voltages, phase currents, and neutral voltage are then measured. The measured voltage and current are used to identify the fault location by using the above-mentioned fault identification method and their results are tabulated in Tables 2.1-2.6. It is mentioned that the value of inductance of the inductor of the compensated network is considered as 6 H.

Table 2.1 Calculation of fault distances for fault resistance 1 Ω

Obs. No.	**Actual faulty section**	**Cal. faulty section**	**Actual, *d***	**Cal., *d* (Existing method)**	**Actual fault dist. (km)**	**Cal. fault dist. (km) (Existing method)**	**Error (%)**
1	6-7	6-7	0.5	0.49	0.64	0.63	1.56
2	9-10	9-10	0.5	0.49	1.53	1.52	0.65
3	32-33	32-33 11-12 34-35	0.25	0.22	2.03	2.01	0.99
4	15-16	15-16	0.5	0.39	2.90	2.88	0.69
5	21-22	21-22	0.5	0.28	4.16	4.12	0.96
6	24-25	24-25 24-39	0.5	0.15	4.72	4.66	1.27

Table 2.2 Calculation of fault distances for fault resistance 10 Ω

Obs. No.	**Actual faulty section**	**Cal. faulty section**	**Actual, *d***	**Cal., *d* (Existing method)**	**Actual fault dist. (km)**	**Cal. fault dist. (km) (Existing method)**	**Error (%)**
1	6-7	6-7	0.5	0.72	0.64	0.66	-3.13
2	9-10	9-10	0.5	0.52	1.53	1.54	-0.65
3	32-33	32-33 11-12 34-35	0.25	0.28	2.03	2.04	-0.49
4	15-16	15-16	0.5	0.53	2.90	2.91	-0.34
5	21-22	21-22	0.5	0.43	4.16	4.15	0.24
6	24-25	24-25 24-39	0.5	0.28	4.72	4.68	0.85

Table 2.3 Calculation of fault distances for fault resistance 30 Ω

Obs. No.	**Actual faulty section**	**Cal. faulty section**	**Actual, *d***	**Cal., *d* (Existing method)**	**Actual fault dist. (km)**	**Cal. fault dist. (km) (Existing method)**	**Error (%)**
1	6-7	7-8 7-28	0.5	0.26	0.64	0.72	-12.5
2	9-10	9-10	0.5	0.60	1.53	1.59	-3.92
3	32-33	32-33 11-12 34-35	0.25	0.47	2.03	2.15	-5.91
4	15-16	15-16	0.5	0.95	2.90	2.98	-2.76
5	21-22	22-23	0.5	0.03	4.16	4.26	-2.40
6	24-25	25-26	0.5	0.67	4.72	4.87	-3.18

Table 2.4 Calculation of fault distances for fault resistance 50 Ω

Obs. No.	**Actual faulty section**	**Faulty section (Existing method)**	**Faulty section (Modified method)**	**Actual fault dist. (km)**	**Fault dist.) (Existing method) (km)**	**Fault dist. (Modified method) (km)**	**Error (%) (Existing Method)**	**Error (%) (Modified)**
1	6-7	7-8	7-8	0.64	0.82	0.70	-28.12	-9.37
2	9-10	9-10	9-10	1.53	1.66	1.64	-8.50	-7.19
3	32-33	32-33 11-12	32-33 11-12	2.03	2.30	2.30	-13.30	-13.30
4	15-16	16-17	16-17	2.90	3.12	3.12	-7.59	-7.59
5	21-22	22-23	22-23	4.16	4.43	4.43	-6.49	-6.49
6	24-25	No converse	23-24	4.87	-----	4.64	------	4.72

Table 2.5 Calculation of fault distances for fault resistance 100 Ω

Obs. No.	**Actual faulty section**	**Faulty section (Existing method)**	**Faulty section (Modified method)**	**Actual fault dist. (km)**	**Fault dist.) (Existing method) (km)**	**Fault dist. (Modified method) (km)**	**Error (%) (Existing Method)**	**Error (%) (Modified)**
1	6-7	8-9	5-6	0.64	0.95	0.60	-48.44	6.25
2	9-10	9-10	9-10	1.53	1.78	1.51	-16.34	1.31
3	32-33	13-14	32-33 11-12 34-35	2.03	2.33	2.05	-14.79	-0.99
4	15-16	17-18	15-16	2.90	3.39	2.95	-16.90	-1.72
5	21-22	25-26	22-23	4.16	4.91	4.49	-18.03	-7.93
6	24-25	No converse	23-24	4.87	-------	4.61	--------	5.34

Table 2.6 Calculation of fault distances for fault resistance 200 Ω

Obs. No.	**Actual faulty section**	**Faulty section (Existing method)**	**Faulty section (Modified method)**	**Actual fault dist. (km)**	**Fault dist.) (Existing method) (km)**	**Fault dist. (Modified method) (km)**	**Error (%) (Existing Method)**	**Error (%) (Modified)**
1	6-7	8-9	6-7	0.64	1.07	0.67	-67.19	-4.69
2	9-10	11-12 32-33 34-35	9-10	1.53	1.89	1.52	-23.53	0.65
3	32-33	No converse	32-33 10-11	2.03	-------	1.97	-------	2.96
4	15-16	19-20	15-16	2.90	3.65	2.84	-25.86	2.07
5	21-22	No converse	21-22	4.16	-------	4.12	--------	0.96
6	24-25	No converse	24-25 24-39	4.87	-------	4.71	--------	3.29

From Tables 2.1-2.6, it is observed that, the accuracy of the above-mentioned existing fault location method for compensated distribution network depends on the fault resistance. Up to the fault resistance, R_f =50 Ω, the accuracy of the obtained fault location is considerable. However, with the further increase of fault resistance such as 100 Ω and 200 Ω, it is observed that, the calculated fault point is sometimes obtained far from the actual faulty section, and thus the error in the calculation of fault location increases significantly. In addition, from Tables 2.3-2.6, it is observed that with increase of fault resistance, the convergence rate is decreasing, i.e., the calculated d is not in the range of $0 < d \leq 1$.

Depending on the inception angle of the voltage phasor at fault point, the neutral current, phase current of faulty phase and voltage across the inductor contain DC components. Fig. 2.9 shows the neutral current with time changing DC component after occurring fault. In this analysis, DC component is ignored so that complex numbers can be used to express the measured voltages and currents. As the DC component is not considered in the expression of voltage and currents, it can be one of the reasons for low accuracy of the existing impedance-based fault location method, especially with increase of fault resistance as mentioned in Tables 2.5 and 2.6. In addition, lumped parameters are used in this analysis instead of distributed parameters, and this can be another reason of the error in the identification of fault location.

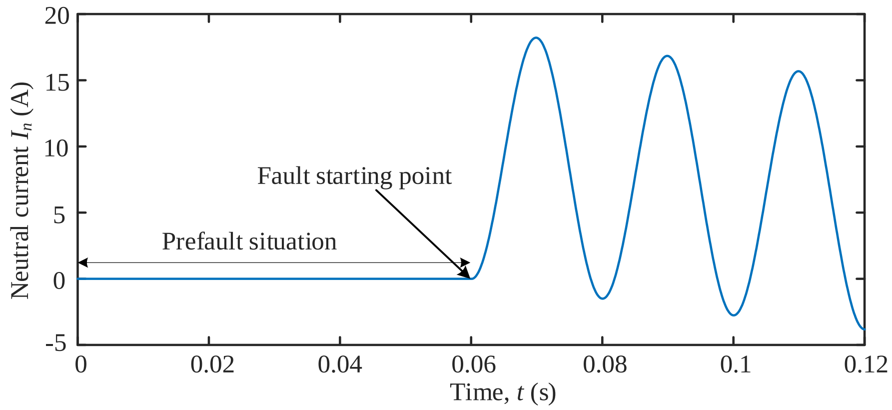

Fig. 2.9 Neutral current of a typical compensated distribution network after occurring single line to ground fault.

To increase the convergence rate of the algorithm of the fault location method, modification is required in the method. As an inductor is connected between the neutral of the substation transformer and ground, the fault current of the compensated network is mainly reactive type. Therefore, the reactive component of the faulty phase plays important role to converge the above-mentioned fault location method. In the proposed modified method, a factor is multiplied in the imaginary part of the calculated faulty phase current which can be mathematically expressed as follows:

$$I_a = I_{ar} + G \times I_{ai} \tag{2.24}$$

where G is the correction factor which depends on the value of fault resistance as shown in Fig. 2.10. The correction factor G is calculated for different fault resistances at various locations until the calculated fault location is near to the action fault point. From (2.5) and (2.23), one can obtain the fault resistance as follows:

$$R_f = \frac{(E'_{an} - V_n)}{I_f} \tag{2.25}$$

where E'_{an} and I_f are obtained by (2.23) and (2.7) respectively.

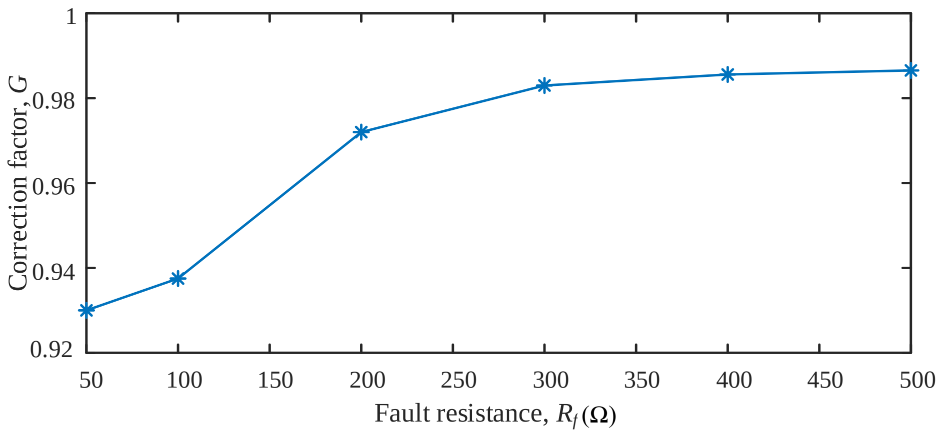

Fig. 2.10 The correction factor with fault resistance for $R_f \geq 50$ Ω.

However, despite of the including of the correction factor, there are some cases where the value d does not remain in the range of $0 < d \leq 1$. In this case, the faulty section is considered where the minimum absolute value of d is obtained, and if the sign of d is negative, the fault point can be considered near to the initial bus of the line section otherwise it is near to the end bus of the section.

In addition, it is also observed from Tables 2.1-2.6 that multiple estimated fault locations are often obtained. To pinpoint fault locations, three possible approaches can be employed which are as follows:

(i) Using measurements of voltages and currents at each branch and sub-branch, which can help to avoid the multiple estimated locations; and

(ii) Identifying the status of circuit breakers at each branch and sub-branch, and their information is then used to select the appropriate fault location.

(iii) Calculate the fault currents separately by impedance-based fault location method and using measured neutral current. After that the fault currents of the corresponding multiple estimated sections are sorted out based on the absolute value of the difference of the real parts of each calculated fault current and fault current obtained by using neutral current.

The above-mentioned first approach to obtain single estimation of fault location by measuring voltages and currents at each branch and sub-branch is quite challenging as the numbers of branches and sub-branches are huge. In the same way, relays of the corresponding circuit breakers do not always operate during the single line to ground fault as the fault current is very small due to the connection of an inductor between neutral of the substation transformer and ground. Therefore, the above-mentioned third way can be possible solution to deal multiple estimations of fault location. As the neutral current is measurable at the substation, the fault current can also be calculated using the neutral current which is as follows:

$$I_{fn} = I_n - I_{cgt} \tag{2.26}$$

with

$$I_{cgt} = I_{acpt} + I_{bcpt} + I_{ccpt} \tag{2.27}$$

where I_{fn} is the fault current obtained using neutral current, and I_{acpt}, I_{bcpt} and I_{ccpt} are the equivalent phase capacitive currents. The currents I_{acpt}, I_{bcpt} and I_{ccpt} are calculated using (2.16) - (2.18), where $X_{cp} = 1/\left(2\pi f \sum C_{pt}\right)$ and $X_{cg} = 1/\left(2\pi f \sum C_{gt}\right)$. The $\sum C_{pt}$ and $\sum C_{gt}$ indicate the total equivalent of C_p and C_g of the whole line.

After considering the above-mentioned modifications such as the correction factor, considering the non-convergence situation, and dealing with multiple estimations, the algorithm of modified impedance-based fault location method can be summarised as follows:

(i) Consider, the fault happens at a point between the buses, i.e., a random value of d ($0 < d \leq 1$) is initially considered.

(ii) Find the voltage at fault point with respect to neutral, E'_{an} by (2.23)

(iii) Calculate the downstream current I_{La} by (2.22).

(iv) Calculate the fault current I_f by (2.7)

(v) Fault distance d is calculated by (2.6).

(vi) If the error between two successive calculated d is within specific limit, then go to step (vii) otherwise go to step (ii).

(vii) Check line section which is not considered for identifying fault location. If available, go to step (i), otherwise go to step (viii).

(viii) Find out the line sections where $0 < d \leq 1$, if obtained go to step (x), otherwise go to (ix)

(ix) Find out the line sections where the minimum absolute value of d is obtained.

(x) Find out the fault resistance using (2.25). If fault resistance is calculated for first time, go to step (xi), otherwise go to step (xiv).

(xi) If the fault resistance greater than 50 Ω, go to step (xii), otherwise go to step (xvi).
(xii) Find out the correction factor.
(xiii) Find out modified faulty phase current by (2.24) and go to step (i).
(xiv) Find out the line sections where $0 < d \leq 1$, if obtained go to step (xvi), otherwise go to (xv)
(xv) Find out the line sections where the minimum absolute value of d is obtained.
(xvi) If single estimation is obtained, then go to step (xviii), otherwise go to step (xvii).
(xvii) Sort out the multiple estimations using the absolute values of the difference of the real parts of I_f and I_{fn}.
(xviii) Stop.

The flow chart of the above-mentioned algorithm for identification of fault location using proposed modified impedance-based method is given in Fig. 2.11.

2.6 Estimation of voltage at fault location

The voltage at fault location can be considered in two ways: one is the voltage with respect to neutral point, and another is the voltage with respect to ground. The estimation of voltage at fault location with respect to neutral point can be obtained by (2.23). On the other hand, the estimation of voltage at fault location with respect to ground can be obtained by the following equation.

$$V_f = E'_{an} - V_n \tag{2.28}$$

In (2.27), the E'_{an} is calculated by (2.23), and V_n is obtained from the measurement.

2.7 Results and discussions

From the Tables 2.1-2.6, it is observed that the accuracy of the conventional impedance-based earth fault location method for compensated distribution network depends on the fault resistance. For low fault resistance, e.g., up to 50 Ω, the accuracy in the calculation in the identification of the fault location can be considered as a considerable range. However, with high fault resistance, the convergence rate as well as the accuracy of the conventional impedance-based fault location method deteriorate drastically. For example, for fault resistance 200 Ω there are some cases as shown in Table 2.6, where no convergence is reached, i.e., the value of d is outside the range of $0 < d \leq 1$. In addition, the error in the calculation of single line to earth fault location rises to more than 23%.

On the other hand, the proposed modified impedance-based fault location identification method improves the convergence rate as well as the accuracy of the method. In addition, there is a provision to deal with cases where the value of d is not in a specific range. Moreover, for multiple estimations, the proposed method sorts them based on the absolute values of the difference of the real parts of I_f and I_{fn}. A single line to ground fault is considered between buses 32 and 33, and three estimation of fault points are obtained for this fault as shown in Table 2.7. The minimum absolute value of the difference of real parts of I_f and I_{fn} is obtained for the line section 32-33 which is the actual faulty section. From the Fig. 2.10, it is observed that the correction factor is considered up to 500 Ω as fault resistance. In the same way, it can be extended to up to several kΩ of fault resistance.

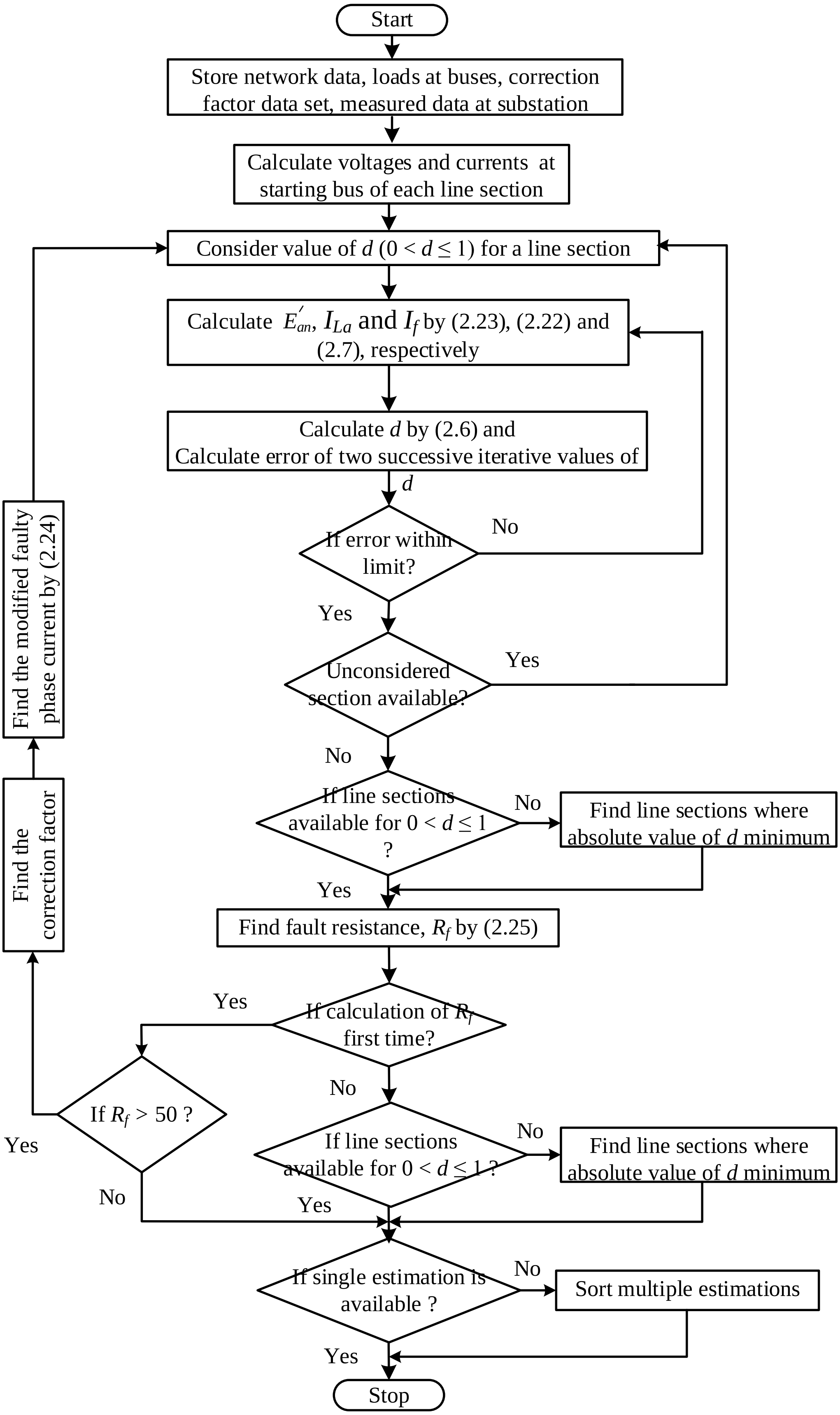

Fig. 2.11 The flow chart of proposed modified impedance-based fault location method.

Table 2.7 Calculated fault currents by the proposed method and using neutral current

Actual faulty section	**Calculated faulty section**	**Fault currents obtained by the proposed method, I_f (A)**	**Fault current using neutral current, I_{fn} (A)**	**Absolute value of differences of real parts of I_f and I_{fn}**
32-33	32-33	0.0612 - 1.4291i	0.0426 - 2.2547i	0.0186
	11-12	0.0614 - 1.4314i		0.0188
	34-35	0.0615 - 1.4316i		0.0189

Table 2.8 Calculation of fault distances for two fault currents at the same fault resistance

Obs. No.	**Actual faulty section**	**Actual fault dist. (km)**	**Fault current about 2.53 A (rms) (L_p=6 H and R_f =500 Ω).**		**Fault current about 0.49 A (rms) (L_p=8.65 H and R_f =500 Ω).**	
			Fault dist. (Modified method) (km)	**Error (%)**	**Fault dist. (Modified method) (km)**	**Error (%)**
1	6-7	0.64	0.58	9.38	0.58	9.38
2	9-10	1.53	1.55	-1.31	1.48	3.27
3	15-16	2.90	2.78	4.14	3.09	-6.55
4	21-22	4.16	3.91	6.01	3.99	4.09

In the above-mentioned analysis, the value of inductance of the inductor coil which is connected between neutral point of substation transformer and ground is considered as 6 H. In this case, the obtained fault current is about 2.53 A (rms) although with change of fault resistance, the fault current changes slightly. To maintain the thermal energy limit (I^2t, where I is the fault current and t is permissible time of fault current) within 0.1 A^2s [11], the fault current needs to be reduced. Table 3.8 shows the results of fault location for the fault current about 0.49 A (rms), where L_p and R_f are considered as 8.65 H and 500 Ω respectively. The corresponding results for fault current about 2.53 A (L_p=6 H) are also shown in Table 2.8. From the Table 2.8, it is observed that the calculation of fault distances is within the acceptable range. It is mentioned that the correction factor for low fault current (I_f =0.49 A) also needs to be determined as the same as the presented in Section 2.5.

Table 2.9 Estimation of voltage at fault location

Obs. No.	**Faulty section**	**Actual (Simulated) E'_{an} (kV)**	**Calculated E'_{an} (kV)**	**Actual (Simulated) V_f (kV)**	**Calculated V_f (kV)**
1	9-10	12.681	12.681	0.131	0.129
2	32-33	12.676	12.674	0.131	0.129
3	15-16	12.671	12.668	0.131	0.128
4	21-22	12.664	12.662	0.131	0.128
5	24-25	12.662	12.660	0.131	0.128

It is observed from Table 2.9 that the estimated voltages at fault locations with respect to the neutral point are close to the actual simulated voltages. In the same way, the calculated voltages with respect to the ground at fault locations are near to the simulated voltages obtained at those locations.

2.8 Appropriateness

The appropriateness of the proposed modified impedance-based fault location method for calculation of fault distances is in the acceptable range as shown in Table 2.3-2.6. Moreover, it is observed from Table 2.8 that there is a good agreement between estimated voltages and simulated voltages at fault location. As the proposed method for identifying the fault location and estimation of voltage at fault location uses the different measured data at substation and line parameters and magnitudes of loads at buses, the accuracy of the method highly depends on those required parameters' measurements.

2.9 Summary

The one of key findings of this chapter is to find out an algorithm based on modified impedance-based fault location method for identifying the fault location for a compensated distribution network. The required data for implementation of the method can be obtained from substation's measurement system. In addition, there is a provision to deal with multiple estimations in the method which can happen due to the branches of the radial network. Moreover, the estimation of voltage at fault location can be obtained by the modified impedance-based fault location method that is another finding of this task.

Chapter 3

Sensitivity Analysis of Different Factors Affecting the Voltage at the Fault Location

3.1 Introduction

To develop an appropriate mechanism for reducing the voltage at fault location and maintaining the thermal energy within the limit, it is essential to investigate the impacts of different factors that affect the voltage at the fault location. There are several factors within the system that affect the voltage at the fault locations, which include inductance of the inductor coil which is connected between neutral point of substation transformer and ground, fault resistance, properties of cables (line capacitance, resistance and inductance), location of fault, loads in the faulty feeder (both magnitude and power factor), fault inception angle, and structures of the network (especially, purely radial or radial with many branches, as in AusNet Services' distribution networks in bushfire-prone areas). In this chapter, the effect of the above-mentioned factors on the voltage at fault location are analysed. In this analysis, MATLAB Simulink platform is used to find out the factors affecting the voltage at fault location as the same as the analysis in Chapter 2. After obtaining the required data, MATLAB program/code is used to show their effects. It is noteworthy that a part of the AusNet's compensated distribution network is used for analysis as presented in Fig. 2.8 of the Chapter 2.

3.2 Intended outcome

A framework needs to be developed to analyse the sensitivity of different factors on the voltage at the fault location. A ranking of these factors is then produced highlighting the severity or contribution of each parameter.

3.3 Factors affecting the voltage at the fault location

There are many factors that are responsible to affect the voltage at fault location such as inductance of the inductor coil, fault resistance, line capacitance, line resistance and line inductance, location of fault, loads in the faulty feeder, fault inception angle, and structures of the network. In the following subsections, each possible factor is analysed based on its contribution on the fault voltage.

3.3.1 Value of inductance of the inductor coil

When a single phase to ground fault occurs in a compensated distribution network as shown in Fig. 2.2, the phase to neutral voltage at the fault location can be expressed as

$$E'_{an} = V_n + I_f R_f \tag{3.1}$$

with

$$V_n = j\omega L_p I_n \tag{3.2}$$

where E'_{an} is the voltage at fault location with respect to neutral, V_n is the voltage across the inductor, and $I_f R_f$ is the voltage across the fault resistance, L_p is the value of inductor, ω is the angular frequency, and I_n is the neutral current. Therefore, the voltage with respect to ground at fault location (V_f), which can be defined as $V_f = R_f I_f$, depends on the inductance value of the inductor coil and fault resistance. To analyse the effect of inductance of the inductor coil on the voltage at fault location, the fault resistance is considered as a constant value, e.g., 100 Ω, and the value of the inductance is changed from low value to high value as shown in Fig. 3.1. From the Fig. 3.1, it is observed that the voltage (peak to peak) with respect to ground ($V_{f(\mathrm{pp})}$) at fault location exponentially reduces with increase of the inductance of the coil. The value of $V_{f(\mathrm{pp})}$ sharply reduces from about 18.5 kV to 4.48 kV by increasing the value of L_p from 0.25 H to 2 H, and after that the voltage goes slowly toward a low value with the further increase of L_p as shown in Fig. 3.1. On the other hand, the voltage (peak to peak) across the inductor coil ($V_{n(\mathrm{pp})}$) increases drastically from 30.38 kV to 35.46 kV due to increase of L_p from 0.25 H to 2 H, and after that the voltage rises slowly towards to phase to neutral voltage with further increase of L_p. The fault current, $I_{f(\mathrm{pp})}$ (peak to peak) reduces with the increase of the inductance of the coil as the same as the voltage at fault location, e.g., the fault currents at 0.25 H and 2 H are 183.29 A and 44.71 A, respectively. In this analysis, instead of conventional root mean square (rms) values of voltage and current, the peak-to-peak values of them are used to avoid the DC effect which may rise in faulty voltage and current after occurring fault.

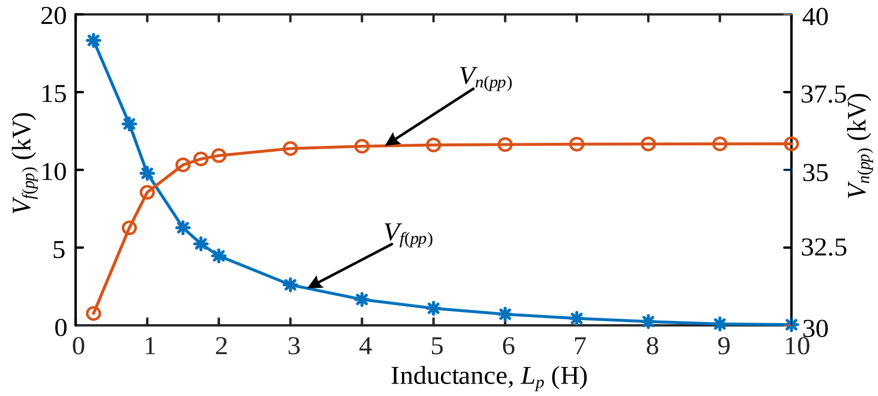

Fig. 3.1 Voltage (peak to peak) at fault location with respect to ground, $V_{f\,(\mathrm{pp})}$ and voltage (peak to peak) across the inductor coil, $V_{n(\mathrm{pp})}$ with change of inductance of the coil.

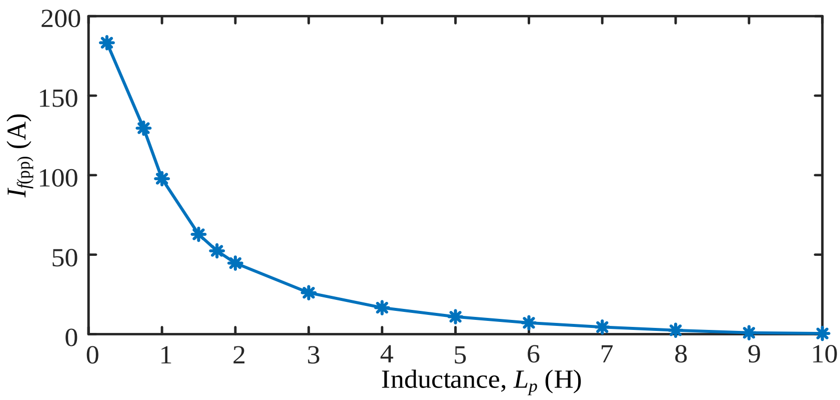

Fig. 3.2 Fault current (peak to peak), $I_{f(\mathrm{pp})}$ with change of inductance of the coil.

3.3.2 Value of fault resistance, R_f

As phase voltage with respect to neutral at fault location is sum of the voltage across the fault resistance and inductor coil as shown in (3.1), the fault resistance plays an important role to fix the fault voltage (with respect to ground) at fault point. To analyse the effect of fault resistance on the voltage at fault location, the value of the inductance of the inductor coil is considered as two discrete values 6 H and 8.65 H, and the value of the fault resistance is changed from low value to high value for each case as shown in Fig. 3.3. From the Fig. 3.3(a), it is observed that in case of L_p=6 H, the voltage from fault point to ground $V_{f(\mathrm{pp})}$ increases gradually with increase of fault resistance, and it goes towards the phase to neutral voltage at fault point. For example, $V_{f(\mathrm{pp})}$ increases from 0.69 kV to 7.05 kV for increase of R_f from 100 Ω to 1000 Ω. On the other hand, there is a decrease trend in the voltage across the inductor coil with increase of the fault resistance, e.g., V_n reduces from 35.84 kV to 35.01 kV for increase of R_f from 100 Ω to 1000 Ω at L_p=6 H as shown in Fig. 3.3(b). However, despite the increase of the voltage from fault point to ground with increase of the fault resistance, the fault current reduces in this case. Up to several hundred of R_f, the fault current reduces very slowly and after that it reduces gradually with increase of R_f. With increase of fault resistance, the total impedance increases between fault point and neutral point of the substation transformer, and consequently the fault current reduces. In the same way, it is observed from Figs. 3.3 and 3.4 that the voltage (peak to peak) at fault location $V_{f(\mathrm{pp})}$, voltage (peak to peak) across the inductor coil $V_{n(\mathrm{pp})}$, and fault current (peak to peak) $I_{f(\mathrm{pp})}$ at L_p=8.65 H change with the fault resistance although these changes occur lower than those for the value of 6 H. In addition, the values of $V_{f(\mathrm{pp})}$ and $I_{f(\mathrm{pp})}$ at L_p=8.65 H are much lower than those at L_p=6 H.

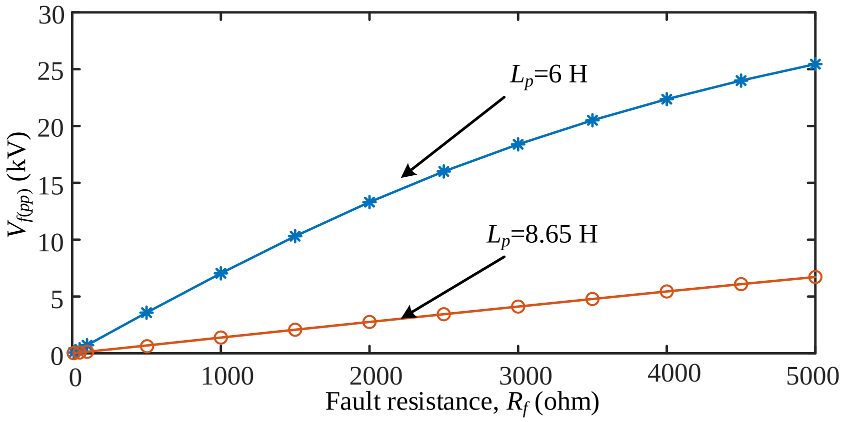

(a)

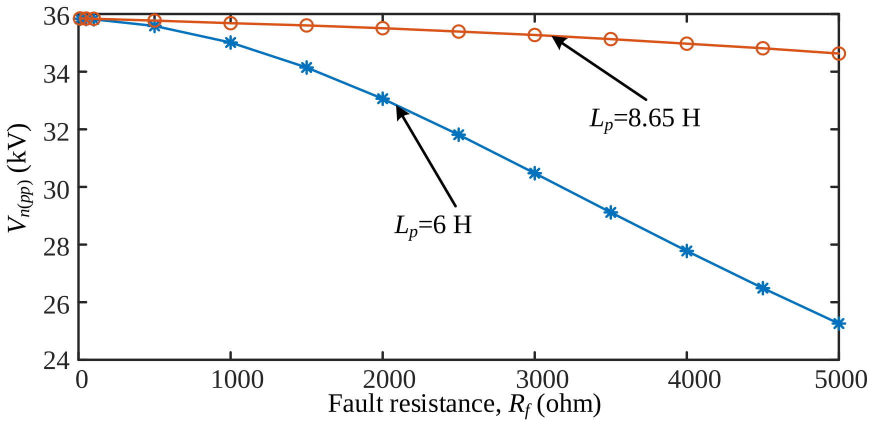

(b)

Fig. 3.3 (a) Voltages (peak to peak) at fault location, $V_{f(pp)}$ with change of fault resistance, R_f at two different values of L_p, and Fig 3.3 (b) voltages (peak to peak) across the inductor coil, $V_{n(pp)}$ with change of fault resistance, R_f at two different values of L_p.

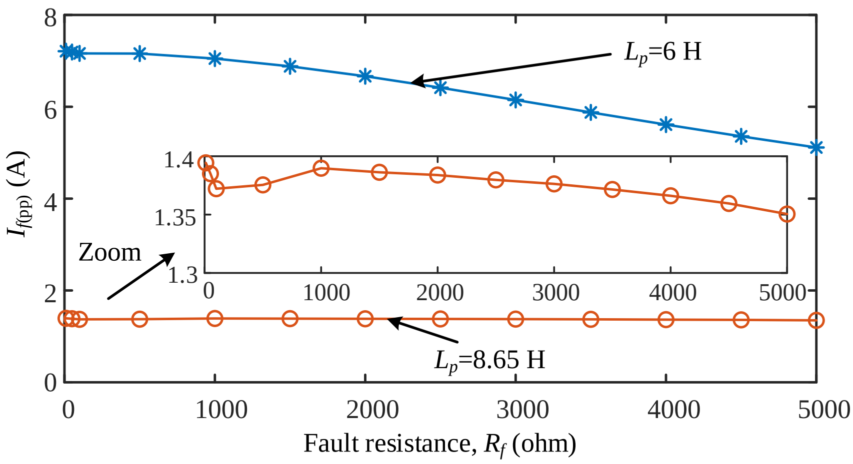

Fig. 3.4 Fault currents (peak to peak), $I_{f(pp)}$ with change of fault resistance, R_f at two different values of L_p

3.3.3 Line capacitance (C_1 and C_0)

Line capacitance, as shown in Fig. 2.5 of Chapter 2, is an important property of the distribution line. After installing the distribution line, the line capacitances (both C_1 and C_0) become generally constant. To understand the effect of the line capacitance on the voltage at fault point, both zero and positive sequence capacitances are increased from its normal situation as shown in Fig. 3.5. From the figure, it is observed that with equally increase of the C_0 and C_1, the voltage at fault location reduces gradually, e.g., with a 15% increase of capacitance from its normal condition, $V_{f(pp)}$ reduces from about 716 V to 539 V. However, after reaching certain point the voltage increases with increase of capacitance. At the minimum point, there exists a resonance condition among the line capacitance and inductance of the inductor coil. In the same way, the fault current reduces gradually with increasing line capacitance, e.g., the $I_{f(pp)}$ reduces from 7.16 A to 5.39 A by 15% increase of the line capacitance from its normal condition as shown Fig 3.6. At the resonance condition, the fault current becomes minimum, and after that it increases with increase of capacitance. In this analysis, the values of the fault resistance and inductance of the inductor coil are considered as 100 Ω and 6 H respectively.

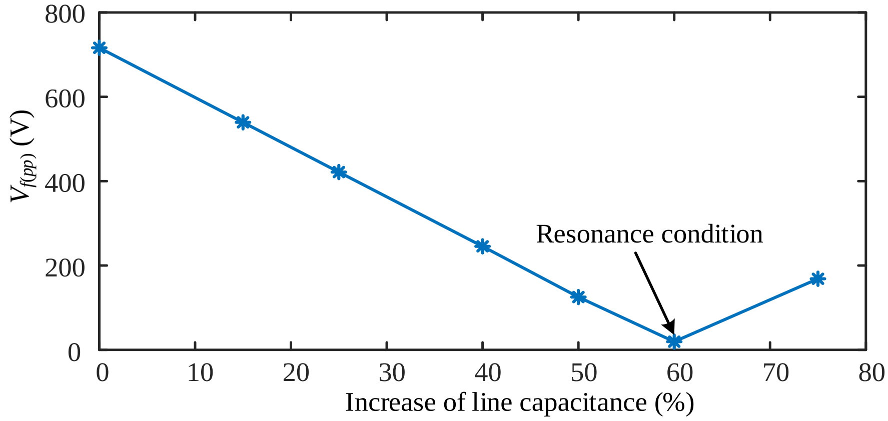

Fig. 3.5 Voltage (peak to peak) at fault location, $V_{f\ (pp)}$ with percentage of increase of the line capacitance.

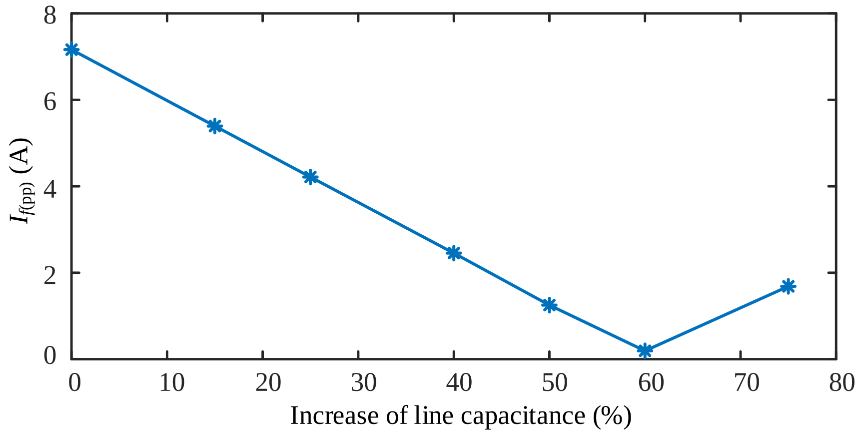

Fig. 3.6 Fault current (peak to peak), $I_{f(pp)}$ with percentage of increase of the line capacitance.

3.3.4 Line resistance and inductance

Line resistance and inductance are also important properties of a distribution line. After installation of the distribution line, the line resistance and inductance are almost constant as the same as the line capacitances. To understand the effect of the line resistance and inductance, (2.5) of Chapter 2 can be rearranged as follows:

$$E_{an} = V_n + I_f R_f + d \times (Z_{aa} I_a + Z_{ab} I_b + Z_{ac} I_c) \tag{3.3}$$

where Z_{aa} is line self-impedance of the line, Z_{ab} and Z_{ac} are mutual impedances of the lines. From (3.3), it is observed that if the impedance of the line changes, the corresponding voltage at fault location changes.

To analyse the effect of the line resistance and inductance, sequence resistances and inductances are equally increased. From the Table 3.1, it is observed that after considering double and triple values of the line resistances and inductances, no significant changes are obtained in the peak-to-peak values of the $V_{f\,(pp)}$ and $I_{f(pp)}$ which remain almost the same values at normal condition.

Table 3.1 $V_{f(pp)}$ and $I_{f(pp)}$ at different line resistance and inductance.

Line resistance and inductance	**(L_p=6 H and R_f=100 Ω).**		**(L_p=8.65 H and R_f=100 Ω).**	
	$V_{f(pp)}$ (V)	**$I_{f(pp)}$ (A)**	**$V_{f(pp)}$ (V)**	**$I_{f(pp)}$ (A)**
Normal	716.3632	7.1636	137.2285	1.3723
Two times	713.9697	7.1397	136.9813	1.3698
Three times	711.4814	7.1148	136.9326	1.3693

3.3.5 Power factor

The change of power factor means the change of line currents I_a, I_b and I_c. From (3.3), it is observed that any change of line currents may affect the voltage at fault location. As the voltage across the inductor, V_n is much greater than voltage across the line, the voltage drop across the line slightly affects the voltage at fault point with respect to ground and fault current as shown in Figs. 3.7 and 3.8. From the figures, both fault voltage and current are almost constants at about 716 V and 7.16 A for 6 H of L_p, and 137.18 V and 1.37 A for 8.65 H of L_P respectively with the increase of the power factor at the same apparent power.

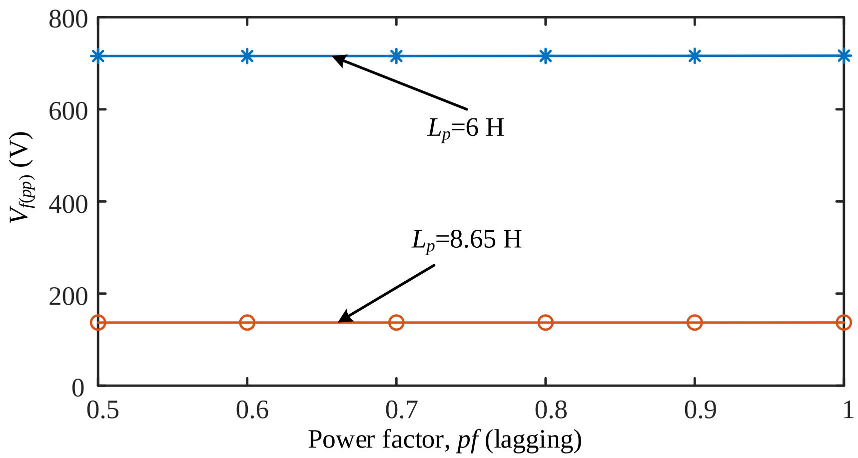

Fig. 3.7 Voltages (peak to peak) at fault location, $V_{f(pp)}$ with increase of power factor at the same VA rating for two different values of L_p (R_f=100 Ω).

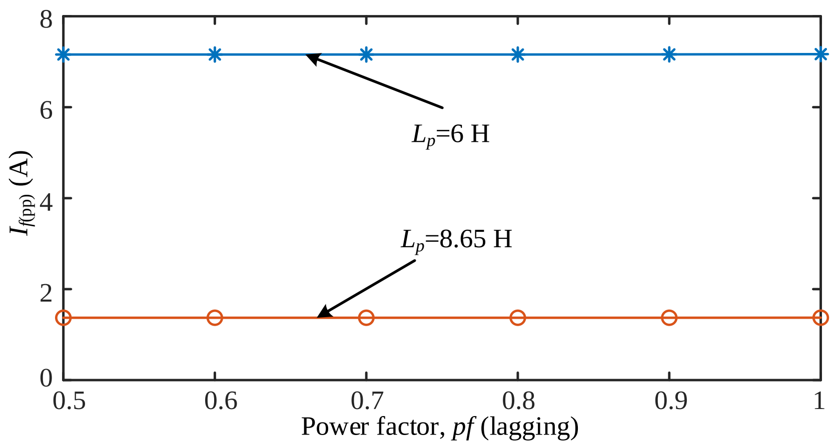

Fig. 3.8 Fault current (peak to peak), $I_{f(pp)}$ with increase of power factor at the same VA rating for two different values of L_p (R_f=100 Ω).

3.3.6 Load magnitude

The effect of the magnitude of load is negligible as with the effect of network power factor. This is true due to the high voltage drop across the inductor coil after a fault occurrence. To analyse the effect of magnitude of the load, each load is connected to the network is increased by two and three times. It is observed from Table 3.2 that after increasing the load magnitude, the values of $V_{f(\mathrm{pp})}$ and $I_{f(\mathrm{pp})}$ do not change significantly especially for the high value of L_p.

Table 3.2 $V_{f(\mathrm{pp})}$ and $I_{f(\mathrm{pp})}$ at different load condition.

Load condition	(L_p=6 H and R_f =100 Ω).		(L_p=8.65 H and R_f =100 Ω).	
	$V_{f(\mathrm{pp})}$ (V)	**$I_{f(\mathrm{pp})}$ (A)**	**$V_{f(\mathrm{pp})}$ (V)**	**$I_{f(\mathrm{pp})}$ (A)**
Normal	716.3632	7.1636	137.2285	1.3723
Two times	714.6736	7.1467	137.2154	1.3722
Three times	713.252	7.1325	137.3890	1.3739

3.3.7 Fault location

The change of fault location means the change of voltage drop across the line between the source and fault point. Therefore, from (3.3), like the effect of change of line impedance the location of fault at the network mildly affects the fault voltage. From Fig. 3.9, it is observed that the voltage with respect to the ground at the fault location remain almost constant with the increase of fault distance for both cases of L_P. In the same way, we can obtain that the fault current is not affected much by the change of fault distance.

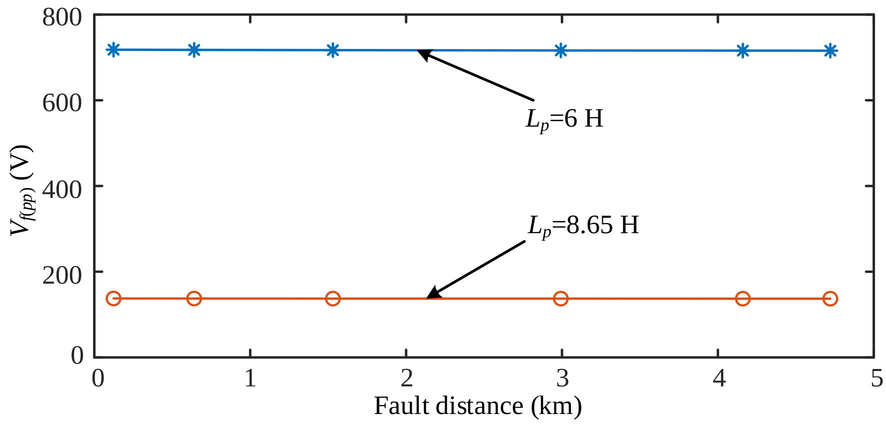

Fig. 3.9 Voltages (peak to peak) at fault location, $V_{f(\mathrm{pp})}$ with increase of distance from substation at two different values of L_p (R_f =100 Ω).

3.3.8 Structures of the network

The distribution network can be purely radial or radial with many branches. However, as the line capacitance increases with a growing number of branches, it has effect on the fault voltage as shown in Fig. 3.5. The above-mentioned network is simulated with and without branches, and the obtained peak to peak voltages at fault location are 716.3632 V and 821.0758 V, respectively for 6 H inductance of inductor coil and 100 Ω fault resistance. In the case of L_p = 8.65 H, the value of the fault voltages with and without branches are 241.8348 V and 137.2285 V, respectively. From the results, it is observed that the voltage at fault location of the network with branches is not equal to that of the network without branches for the same value of L_p. It happens because the equivalent capacitance of a network changes with addition of branches.

3.3.9 Fault inception angle

In this case, fault inception angle is defined as the position of voltage waveform at which earth fault occurs. The voltage at fault location and fault current are slightly affected by the fault inception angle as shown in Table 3.3.

Table 3.3 $V_{f(pp)}$ and $I_{f(pp)}$ at different fault inception angles.

Fault inception angle	**(L_p=6 H and R_f =100 Ω).**		**(L_p=8.65 H and R_f =100 Ω).**	
	$V_{f(pp)}$ (V)	**$I_{f(pp)}$ (A)**	**$V_{f(pp)}$ (V)**	**$I_{f(pp)}$ (A)**
0°	715.1238	7.1512	137.3893	1.3739
36°	716.3632	7.1636	137.2274	1.3723
72°	719.3485	7.1935	138.5749	1.3858

3.4 Discussions

From the above discussions, it is observed that the value of inductance of inductor, fault resistance and line capacitance play important roles in the value of fault voltage at the fault location. As the line capacitance or structure of network is generally fixed after installation of network, the value of inductance and fault resistance are affecting the line voltage at the fault location significantly. In addition, as fault resistance is unknown, the inductance of the inductor coil is mainly varied to fix the voltage at fault location as well as fault current. Other parameters such as fault location, line resistance, inductance, load, and fault inception angle have negligible effect on the voltage at fault location and fault current, especially for the high value of L_P. At the high value of L_p, it is possible to get low value of fault current. For example, the rms value of the fault current for the considered network is about 0.49 A (1.37 A, peak-to-peak value) at L_p =8.65 H and R_f= 100 Ω. Due to the small amount of fault current, many factors such as fault location, line resistance, inductance, load, and fault inception angle have negligible effect on the voltage at fault location. It is worth noting that for minimising the risk of bushfires, the fault current needs to be small so that it maintains the thermal energy limit within 0.1 A^2s.

3.5 Appropriateness

The sensitivity analysis of different factors affecting the voltage at fault location is justified by both theorical explanation and simulated analyses. Therefore, the appropriateness of the analysis maintains a good agreement between theorical explanation and simulated analysis.

3.6 Summary

In this chapter, different factors affecting the voltage at fault location are identified based on both the theoretical and simulated analyses. The value of inductance of the inductor and fault resistance are significant factors to fix the voltage at fault location. The value of line capacitance also plays considerable effect on the voltage at fault location. Addition of a branch with a network can affect the fault voltage as the total equivalent line capacitance increases in this case. Other factors such as fault location, line resistance, line inductance, load, and fault inception angle have negligible effect on the voltage at fault location, especially at high value of inductance of the inductor.

Chapter 4

Development of an Adaptive Approach for Calculating the Network Damping Based on the Real-time Measurement

4.1 Introduction

For assessing the operation of REFCL devices, the network damping is a very important index as it indicates the amount of leakage currents to ground across the network. The higher leakage currents in the network, the larger damping of the network. As such, the value of the network damping is directly proportional to the sensitivity of the REFCL, since the ability of REFCL to detect low fault currents depends on the minimisation of the leakage currents.

The objective of the task is to estimate the damping from measurements at different points of the REFCL protected electrical power distribution network. When the network is reconfigured, e.g., by rearranging a zone substation, adding a new zone substation, or rearranging feeders, we need to able to find out the impact on network damping. It is worthwhile to stress that, the estimation should be based calculation along with measurements. We know that the damping depends on capacitance C_0 and resistance R_0. In terms of capacitance, there is no impact of network reconfiguration. All capacitances of different cable segments are added up to find out C_0. In terms of the balancing program the error of 5 – 10mA are found in each section, but that is within the tolerance level of AusNet. From power flow analysis, Sincal can report C_0, but the finding of R_0 needs further investigation.

Previous analysis showed that damping was bad when there are open conductors at the beginning and cable at the end. Moreover, the series and parallel configuration also had impact on damping. So, the following needs to be investigated:

- Investigate how you will calculate the value of R_0 theoretically or from measurements?
- Is R_0 dependent on network configuration?

Next the equivalent circuit model is proposed that can be used to estimate damping in the REFCL protected network from measurements.

4.2 Relation of network damping with circuit parameters

To calculate the main parameters of the compensated networks, the equations that represent such networks are derived in this section. The transmission systems are represented as a shunt capacitor (C_A, C_B, and C_C for phases A, B and C respectively). The losses in the transmission systems are represented as shunt resistors (R_{GA}, R_{GB} and R_{GC}) as shown in Fig. 4.1. Petersen coil in the neutral point is represented as inductance L_p (the losses in the coil are not considered in this analysis).

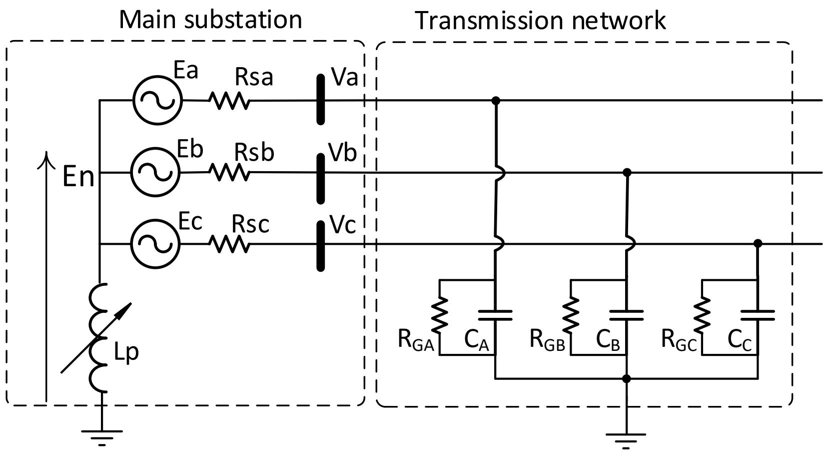

Fig. 4.1 Equivalent circuit of a compensated network

In normal condition, the following set of equations can be derived based on Fig. 4.1 (The source resistances R_{sa}, R_{sb} and R_{sc} are relatively small and not included).

$$V_a\,Y_a \;+\; V_b\,Y_b \;+\; V_c\,Y_c \;=\; -E_n\,Y_p \tag{4.1}$$

where V_a, V_b and V_c are the phase to ground voltages of phases A, B and C respectively, E_n is the neutral to ground voltage, and the admittances Y_a, Y_b, Y_c and Y_p are defined as

$$Y_x = \left(\frac{1}{R_{Ex}}\right) + j\omega C_X = G_{Gx} + jB_{Cx} \tag{4.2}$$

where the subscript x denotes the phases a, b or c, ω is the angular frequency of the network, G_{Gx} and B_{Cx} are the conductance and susceptance of phase x respectively, j $= \sqrt{-1}$,and $Y\_p = \; -j/\omega L_p$, where L_p is the inductance of the REFCL.

The relationship between the phase to neutral and phase to ground voltages in Fig. 4.1 can be represented as

$$\left.\begin{aligned} V_a &= E_a + E_n \\ V_b &= E_b + E_n \\ V_c &= E_c + E_n \end{aligned}\right\} \tag{4.3}$$

where V_a, V_b and V_c are the phase to ground voltages of phases A, B and C respectively, E_a, E_b and E_c are the phase to neutral voltages and E_n is the neutral to ground voltage.

From (4.1) and (4.3), the neutral voltage can be represented as

$$E_n = -\,\frac{Y_a\,E_a + Y_b\,E_b + Y_c\,E_c}{Y_a + Y_b + Y_c + Y_p} \tag{4.4}$$

If a symmetrical voltage system is considered, the phase to neutral voltages will be related to each other as

$$\left.\begin{aligned} E_a &= V_{ph}\angle 0 &&= V_{ph} \\ E_b &= V_{ph}\angle -120^\circ &&= a^2 V_{ph} \\ E_c &= V_{ph}\angle +120^\circ &&= a\, V_{ph} \end{aligned}\right\} \tag{4.5}$$

where, V_{ph} is the rated phase to neutral voltage and $a = e^{j120^\circ}$. Thus, the neutral voltage in compensated networks becomes

$$E_n = -V_{ph}\frac{Y_a + a^2 Y_b + aY_c}{Y_a + Y_b + Y_c + Y_p} \tag{4.6}$$

Expanding the admittances and rearranging (4.6) to get

$$E_n = V_{ph}\frac{k_r + k_c}{m + j\,d} \tag{4.7}$$

where, k_r and k_c are complex factors represent the asymmetry in the lumped leakage resistance and the lumped shunt capacitance of the compensated networks. They are defined as

$$k_c = \frac{C_A + a^2 C_B + a\, C_C}{C_A + C_B + C_C} \tag{4.8}$$

$$k_r = \frac{G_{GA} + a^2 G_{GB} + a\, G_{GC}}{j\omega(C_A + C_B + C_C)} \tag{4.9}$$

The accurate value of the asymmetry factor, k, is defined as

$$k = k_c + k_r \tag{4.10}$$

However, in the practical measurements of REFCL, k_r is ignored and the value of k_c in (4.8) is used.

The factor m in (4.7) is the resonance mismatch (or detuning) factor of the REFCL and it is calculated as

$$m = \frac{1}{\omega L_p \times \omega(C_A + C_B + C_C)} - 1 \tag{4.11}$$

Moreover, a quantitative measure of the damping is obtained by a damping coefficient d calculated as

$$d = \frac{G_\mathrm{A} + G_\mathrm{B} + G_\mathrm{C} + G_0}{B_\mathrm{A} + B_\mathrm{C} + B_\mathrm{C}} \tag{4.12}$$

Next an adaptive approach is proposed that can be used to estimate network damping.

4.3 Adaptive method for generalised non-linear system

The generalized non-linear system is srepresented as follows:

$$\dot{x} = f(x)\theta + g(x)u + d \tag{4.13}$$

where u is the control input, θ is the unknown parameter that needs to be estimated and d is the disturbance. The control objective is to make the state variable x to follow the desired trajectory, x_d. The error is the system is as follows:

$$e = x - x_d \tag{4.14}$$

Hence, the dynamics of error can be represented as follows:

$$\dot{e} = \dot{x} - \dot{x_d} = f(x)\theta + g(x)u + d - \dot{x_d} \tag{4.15}$$

where the value of $\dot{x}$ is substituted from (4.13). Now, let the estimated value of the unknown parameter θ is represented by $\hat{\theta}$. Hence, the error in estimated would be $\tilde{\theta} = \theta - \hat{\theta}$. Replacing the value of θ in (15), we obtain:

$$\dot{e} = \dot{x} - \dot{x_d} = f(x)(\tilde{\theta} + \hat{\theta}) + g(x)u + d - \dot{x_d} \tag{4.16}$$

The stability of the system can be analysed by using the following Lyapunov function:

$$W = \frac{1}{2}e^2 + \frac{1}{2\gamma}\tilde{\theta}^2 \tag{4.17}$$

When $\dot{W} \leq 0$, $\dot{e}$ will be stable, i.e., the error is minimized with $e \to 0$. Thus, we get

$$\dot{W} = e\dot{e} = e\left[f(x)(\tilde{\theta} + \hat{\theta}) + g(x)u + d - \dot{x_d}\right] + \frac{1}{\gamma}\tilde{\theta}\dot{\tilde{\theta}} \tag{4.18}$$

which is simplified as follows:

$$\dot{W} = e\left[f(x)\hat{\theta} + g(x)u + d - \dot{x_d}\right] + \frac{1}{\gamma}\tilde{\theta}(-\dot{\hat{\theta}} - \gamma f(x)e) \tag{4.19}$$

If θ is initially chosen as constant, the change of θ, $\theta = 0$ which gives, $-\dot{\tilde{\theta}} = \dot{\hat{\theta}}$ as $\tilde{\theta} = \theta - \hat{\theta}$. Hence, we obtain the following:

$$\dot{W} = e\left[f(x)\hat{\theta} + g(x)u + d - \dot{x_d}\right] + \frac{1}{\gamma}\tilde{\theta}(\dot{\hat{\theta}} - \gamma f(x)e) \tag{4.20}$$

If the following condition holds the estimation error can be eliminated:

$$\dot{\hat{\theta}} = \gamma f(x)e \tag{4.21}$$

Thus,

$$\dot{W} = e\left[f(x)\hat{\theta} + g(x)u + d - \dot{x_d}\right] \tag{4.22}$$

The control input will have unknown disturbance if $f(x)\hat{\theta} + g(x)u + d - \dot{x_d} = -ke$. The following approach needs to be used:

$$\dot{W} = e\left[f(x)\hat{\theta} + g(x)u + d - \dot{x_d} + F_B sgn(z) - F_B sgn(z)\right] \tag{4.23}$$

Thus

$$\dot{W} = e\left[f(x)\hat{\theta} + g(x)u - \dot{x_d} + F_B sgn(z)\right] + e[d - F_B sgn(z)] \tag{4.24}$$

where

$$sgn(z) = \begin{cases} +1 \text{ if } z > 0 \\ 0 \quad \text{if } z = 0 \\ -1 \text{ if } z < 0 \end{cases} \tag{4.25}$$

If the following conditions in (4.24) and (4.25) hold, $\dot{W}$ will be less than or equal to 0:

$$d - F_B sgn(z) = 0 \text{ or } d = F_B sgn(z) \tag{4.26}$$

And

$$f(x)\hat{\theta} + g(x)u - \dot{x_d} + F_B sgn(z) = -ke \tag{4.27}$$

Hence, the disturbance can be bounded as:

$$|\varepsilon| \leq F_B \tag{4.28}$$

The original control signal is selected as follows:

$$u = -\frac{1}{g(x)}[f(x)\hat{\theta} - \dot{x_d} + ke + F_B sgn(z)] \tag{4.29}$$

Based on the theory, a dynamical model of the REFCL network is created in next section that will enable controlling the damping.

4.4 Dynamic model of REFCL network

The dynamical model of an arc suppression device (ASD) in resonant grounded power distribution systems can be written as [9, 12, 13, 14]:

$$\frac{dv_N}{dt} = \frac{1}{3C_0} i_N - \frac{v_f}{3C_0 R_f} + \frac{1}{C_0 R_0} v_N \tag{4.30}$$

$$\frac{di_N}{dt} = \frac{1}{L_p}(mV_{dc} - v_N) \tag{4.31}$$

where a fault in phase A is applied in the resonant grounded power distribution systems as shown in Fig. 4.2.

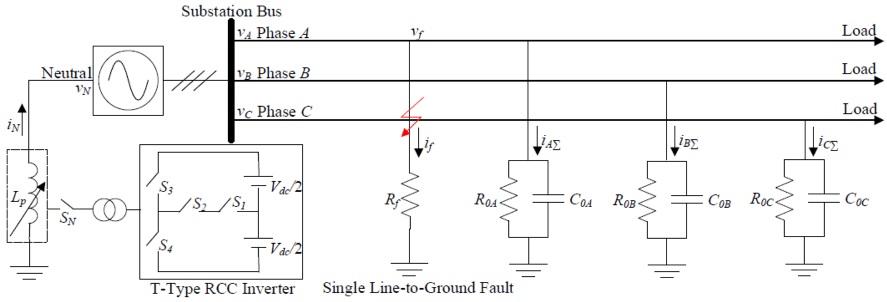

Fig. 4.2 Equivalent model of a faulted resonant grounded power distribution network [9, 12]

If it is assumed the distribution system is balanced, then $R_{0A} = R_{0B} = R_{0C} = R_0$ and

$C_{0A} = C_{0B} = C_{0C} = C_0$. Practically, it is very complicated to measure the value of the parameters C_0, R_0, and L_p. Therefore, these parameters can be considered as unknown during the design of a controller. Hence, if C_0, R_0, and L_p are considered as unknown parameters then the following terms can be obtained:

$$\theta_1 = \frac{1}{3C_0}, \theta_2 = \frac{1}{C_0 R_0}, \text{ and } \theta_3 = \frac{1}{L_p} \tag{4.32}$$

Using the terms from equation (4.32), equations (4.30) and (4.31) can be rewritten as follows:

$$\frac{dv_N}{dt} = \theta_1(i_N - \frac{v_f}{R_f}) + \theta_2 v_N \tag{4.33}$$

$$\frac{di_N}{dt} = \theta_3(mV_{dc} - v_N) \tag{4.34}$$

In the following section, the proposed controller will be designed based on the model with parameter variations as described by equations (4.33) and (4.34).

4.5 Fault compensator and parameter estimator design for the REFCL network

In this section, to mitigate the fault current due to single phase-to-ground faults, the control law m is designed to track the reference trajectory v_N and i_N, respectively. The proposed adaptive backstepping sliding mode controller is designed to achieve this objective which is elaborately described in the following step-by-step.

Step 1- Tracking the neutral voltage: For the v_N tracking objective, the tracking error, e_1 can be defined as follows:

$$e_1 = v_N - v_{N(ref)} \tag{4.35}$$

The dynamic of e_1 using equation (4.33) can be written as:

$$\frac{de_1}{dt} = \theta_1\left(i_N - \frac{v_f}{R_f}\right) + \theta_2 v_N - \frac{dv_{N(ref)}}{dt} \tag{4.36}$$

In terms of estimation errors, equation (4.36) can be written as:

$$\frac{de_1}{dt} = (\hat{\theta}_1 + \tilde{\theta}_1)\left(i_N - \frac{v_f}{R_f}\right) + (\hat{\theta}_2 + \tilde{\theta}_2)v_N - \frac{dv_{N(ref)}}{dt} \tag{4.37}$$

where $\tilde{\theta}_i = \theta_i - \hat{\theta}_i$ with $i = 1, 2$ is the estimation error and $\hat{\theta}_i$ is the estimation of the unknown parameter θ_i. At this stage, to stabilize the v_N tracking error, the control Lyapunov function (CLF) can be chosen as follows:

$$W_1 = \frac{1}{2}e_1^2 + \frac{1}{2\gamma_1}\tilde{\theta}_1^2 + \frac{1}{2\gamma_2}\tilde{\theta}_2^2 \tag{4.38}$$

where γ_i with $i = 1,2$ is an adaptation gain parameter.

The derivative of W_1 is

$$\dot{W}_1 = e_1\left[\hat{\theta}_1\left(i_N - \frac{v_f}{R_f}\right) + \hat{\theta}_2 v_N - \frac{dv_{N(ref)}}{dt}\right] - \frac{1}{\gamma_1}\tilde{\theta}_1\left[\dot{\hat{\theta}}_1 - \gamma_1 e_1\left(i_N - \frac{v_f}{R_f}\right)\right] - \frac{1}{\gamma_2}\tilde{\theta}_2[\dot{\hat{\theta}}_2 - \gamma_2 e_1 v_N] \tag{4.39}$$

At this stage, the virtual control law for the stabilizing function i_N can be selected as follows:

$$\alpha = \frac{1}{\hat{\theta}_1}[\hat{\theta}_1\frac{v_f}{R_f} - \hat{\theta}_2 v_N + \frac{dv_{N(ref)}}{dt} - k_1 e_1] \tag{4.40}$$

where $k_1 > 0$

Moreover, the adaptation laws can be selected as:

$$\dot{\hat{\theta}}_1 = \gamma_1 e_1\left(i_N - \frac{v_f}{R_f}\right) \tag{4.41}$$

$$\dot{\hat{\theta}}_2 = \gamma_2 e_1 v_N \tag{4.42}$$

However, in order to avoid the over parameterization, the adaptation laws as presented by equations (4.41) and (4.42) are not used in this step, instead of parameter tunning functions can be defined as follows:

$$\tau_1 = \gamma_1 e_1\left(i_N - \frac{v_f}{R_f}\right) \tag{4.43}$$

$$\tau_2 = \gamma_2 e_1 v_N \tag{4.44}$$

Using equations (4.40), (4.43), and (4.44), equation (4.39) can be simplified as follows:

$$\dot{W}_1 = -k_1 e_1^2 - \frac{1}{\gamma_1}\tilde{\theta}_1\left[\dot{\hat{\theta}}_1 - \tau_1\right] - \frac{1}{\gamma_2}\tilde{\theta}_2[\dot{\hat{\theta}}_2 - \tau_2] \tag{4.45}$$

Now, the derivative of α is calculated in this step as it will be essential in the next step and it is

$$\dot{\alpha} = M_1 - \theta_1 P_1 - \theta_2 P_2 \tag{4.46}$$

where

$M_1 = M - N - \frac{k_1}{\hat{\theta}_1^2}\dot{v}_{N(ref)}$,
$M = \frac{1}{\hat{\theta}_1^2}(\frac{v_f}{R_f}\dot{\hat{\theta}}_1 + \hat{\theta}_1\frac{d}{dt}i_f - \dot{\hat{\theta}}_2 v_N - \ddot{v}_{N(ref)})$,
$N = \frac{1}{\hat{\theta}_1^2}(\frac{v_f}{R_f}\hat{\theta}_1 - \hat{\theta}_2 v_N + \dot{v}_{N(ref)} - k_1 e_1)\dot{\hat{\theta}}_2$,
$P_1 = \frac{1}{\hat{\theta}_1^2}(i_N - \frac{v_f}{R_f})(\hat{\theta}_2^2 + k_1)$, and
$P_2 = \frac{1}{\hat{\theta}_1^2}(\hat{\theta}_2^2 + k_1)v_N$.

Step 2 - Tracking the neutral current: For the i_N tracking objective, the tracking error, e_2 can be defined as follows:

$$e_2 = i_N - \alpha \tag{4.47}$$

The derivative of e_2 is

$$\dot{e}_2 = \theta_3(mV_{dc} - v_N) - M_1 + \theta_1 P_1 + \theta_2 P_2 \tag{4.48}$$

In terms of estimation errors, (4.48) can be rewritten as:

$$\dot{e}_2 = (\hat{\theta}_3 + \tilde{\theta}_3)(mV_{dc} - v_N) - M_1 + (\hat{\theta}_1 + \tilde{\theta}_1)P_1 + (\hat{\theta}_2 + \tilde{\theta}_2)P_2 \tag{4.49}$$

Now, the final CLF is selected as follows:

$$W_2 = W_1 + \frac{1}{2}e_2^2 + \frac{1}{2\gamma_3}\tilde{\theta}_3^2 \tag{4.50}$$

The derivative of W_2 is

$$\begin{aligned}\dot{W}_2 = -k_1 e_1^2 + e_2\big[\hat{\theta}_3(mV_{dc} - v_N) - M_1 + \hat{\theta}_1 P_1 + \hat{\theta}_2 P_2\big] \\ - \frac{1}{\gamma_1}\tilde{\theta}_1\left[\dot{\hat{\theta}}_1 - \tau_1 - \gamma_1 e_2 P_1\right] \\ - \frac{1}{\gamma_2}\tilde{\theta}_2\left[\dot{\hat{\theta}}_2 - \tau_2 - \gamma_2 e_2 P_2\right] \\ - \frac{1}{\gamma_3}\tilde{\theta}_3\left[\dot{\hat{\theta}}_3 - \gamma_3 e_2(mV_{dc} - v_N)\right]\end{aligned} \tag{4.51}$$

At this stage, the control law and adaptation laws can be selected as follows:

$$m = -\frac{1}{\hat{\theta}_3 V_{dc}}[-v_N\hat{\theta}_3 - M_1 + \hat{\theta}_1 P_1 + \hat{\theta}_2 P_2 + k_2 e_2] \tag{4.52}$$

$$\dot{\hat{\theta}}_1 = \tau_1 + \gamma_1 e_2 P_1 \tag{4.53}$$

$$\dot{\hat{\theta}}_2 = \tau_2 + \gamma_2 e_2 P_2 \tag{4.54}$$

$$\dot{\hat{\theta}}_3 = \gamma_3 e_2(mV_{dc} - v_N) \tag{4.55}$$

Finally, equation (4.51) reduces to

$$\dot{W}_2 = -k_1 e_1^2 - k_2 e_2^2 \leq 0 \tag{4.56}$$

In the next step, some simulation results will be presented based on test case network.

4.6 Simulation on adaptive prediction

Here an adaptive prediction mechanism has been developed to predict C_0 and R_0 in the compensated distribution network. Some preliminary simulations, based on the parameters given in Table 4.1 [13, 14], are done to check the effectiveness of the proposed method which are presented below.

Fig. 4.3 shows the estimation of zero-sequence resistance, R_0 based on different network conditions. Different fault scenarios are simulated and the estimated zero-sequence resistance,

R_0 is approximately 28 kΩ. The prediction mechanism can estimate the zero-sequence resistance with very high accuracy for fault resistance up to 10 kΩ. For fault resistance of 25.4 kΩ, the prediction accuracy is slightly lower. This is due to the fact that the controller is designed for a large dynamic range of fault resistance, hence some errors are expected to occur at the boundary. However, this limitation can be overcome by using intelligent gain tuning algorithm, for example, machine learning or artificial neural network to provide more accurate estimation of network parameters.

Table 4.1 Simulation parameters [13, 14]

Parameters	**Values**
L_p	0.9 H
R_f	50 Ω – 25.4 kΩ
Nominal load resistance per phase	400 Ω
Phase-to-neutral voltage	12.7 kV (rms)
Phase-to-ground voltage	12.7 kV (rms)
Line-to-line voltage	22 kV
$V_{dc}/2$	400 V

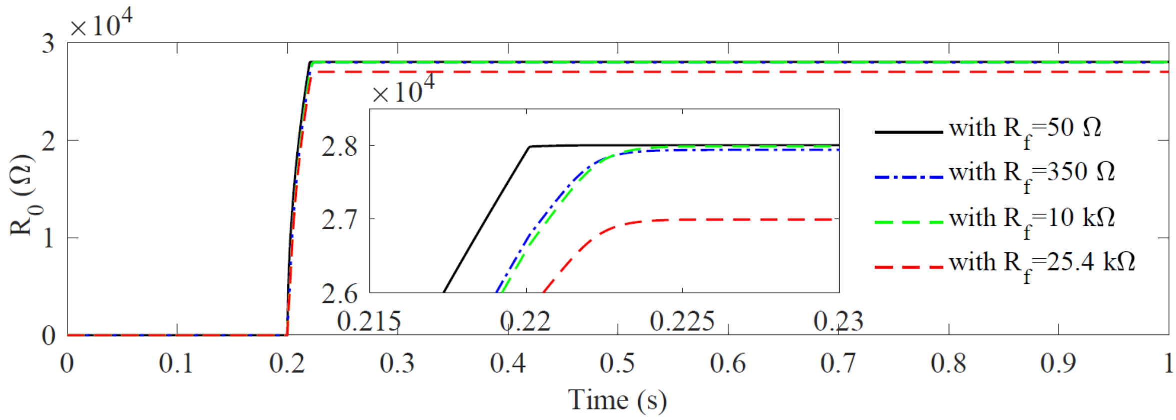

Fig. 4.3 Estimation of zero sequence resistance R_0 for different fault resistances

Similar results are shown in Fig. 4.4 for the prediction of zero-sequence capacitance, C_0 which is estimated to be around 4 μF. Similar to the previous case, the prediction accuracy varies within a reasonable limit. However, this accuracy can be improved by selecting appropriate intelligent controller gain tuning algorithm, which is a future direction for research.

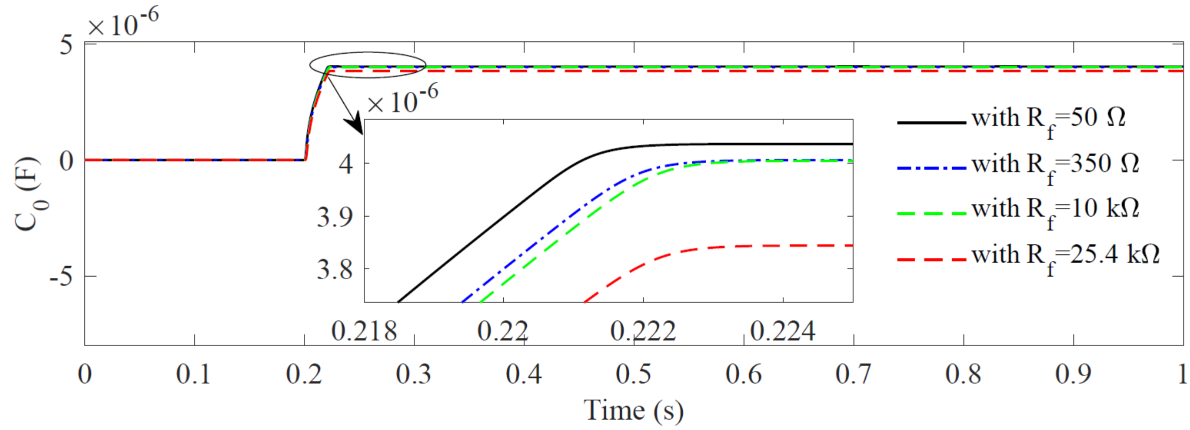

Fig. 4.4 Estimation of zero sequence resistance C_0 for different fault resistances

In the previous simulations, the inductance (L_p) is assumed to be known. To cross-check the validity of this research, another simulation is carried out where the inductance is estimated based on network measurements as shown in Fig. 4.5. The accuracy of this estimation is comparable to previous estimations.

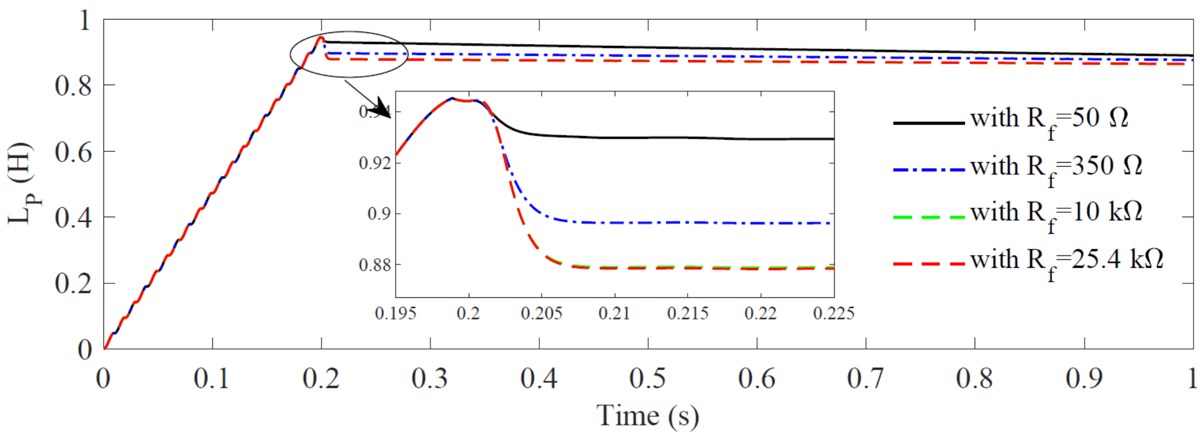

Fig. 4.5 Estimation of L_P for different fault resistances

In the next section, the impact of network reconfiguration on network damping has been investigated.

4.7 Simulation on network reconfiguration

The impact of network reconfiguration in damping has been investigated in this section by using Sincal network model for one of the resonant grounded networks of AusNet Services. A damping calculator has been developed and calculated damping is compared with measurement data in the substations. Table 4.2 shows damping comparison for several AusNet Services distribution network.

Table 4.2 Comparison of damping in AusNet Services network

Sub	R0	X0	Damping % (Calculated)	Damping % (Measured)
KLK	67.2030	-776.2700	8.66	5.48
WYK	6.7430	192.1400	3.51	3.85

Furthermore, network elements are randomly removed from the network and damping is calculated in the network. It was found that, distribution feeders that span long distance have more impact on damping than short feeders. Moreover, cables have significant impact of damping than overhead cables. AusNet Services have been working on updating Sincal network models to reflect changes incurred during REFCL commissioning. More analysis will be carried out as network models become available to devise proper network reconfiguration strategy.

4.8 Discussion on objectives, deliverables and intended outcomes

An adaptive approach has been developed that can estimate zero-sequence component of the REFCL compensated distribution network based on neutral current and voltage measurements. The proposed method accurately predicts zero-sequence parameters. Simulation results show that the network damping depends on the length of the distribution line and presence of underground cables. Development of network reconfiguration scheme needs to consider the optimal placement of underground cables. However, more simulation needs to be carried out on updated network models to get better understanding of the impact of various network parameters on damping.

4.8 Future outlook

Inclusion of intelligent gain tuning method in the proposed controller would effectively increase the accuracy of the proposed method which is a future research direction to consider.

Chapter 5
Analyse the Impacts of Sub-transmission Lines on the Network Imbalance of Distribution Lines Due to Sharing the Same Pole

5.1 Introduction

In AusNet Services REFCL networks, several 22-kV feeders share poles with 66-kV lines. It was found that the 66-kV lines have a significant impact on the unbalance current at 22-kV feeders if they share the same poles (or run in parallel to each other with minimal distance). Especially, the change in the unbalance current was observed while switching the 66-kV line. On the other hand, REFCL devices are sensitive to unbalance current for detecting faults in the network. Therefore, it is required to investigate the actual relationship between the unbalance current at the 22-kV feeder and the 66-kV line parameters. This report includes a mathematical model indicating the relationships between the unbalance current at the 22-kV feeder with the following parameters of both 22-kV and 66-kV lines: phase voltages, line currents, and overhead line parameters, such as types of conductors, heights from the ground, spacing between conductors, length of sharing, etc.

5.2 Unbalance current at the 22-kV feeder

The unbalance current at the 22-kV feeder, as shown in Fig. 5.1, can be represented as follows:

$$I_n = j\omega\left(V_{rg}C_{rg} + V_{wg}C_{wg} + V_{bg}C_{bg}\right) \tag{5.1}$$

where V_{rg}, V_{wg}, and V_{bg} are the phase-to-ground voltages of the three phases of the 22-kV distribution network; C_{rg}, C_{wg}, and C_{bg} are the capacitances from the three phases to the ground of the 22-kV distribution network; ω is the angular frequency; and I_n is the unbalance neutral current. We need to develop a method to estimate C_{rg}, C_{wg}, and C_{bg}. Now, due to the vicinity of 66-kV line with the 22-kV line, there will be an impact of the 66-kV line on the 22-kV line. But first, let us focus on the case where the 66-kV line is absent.

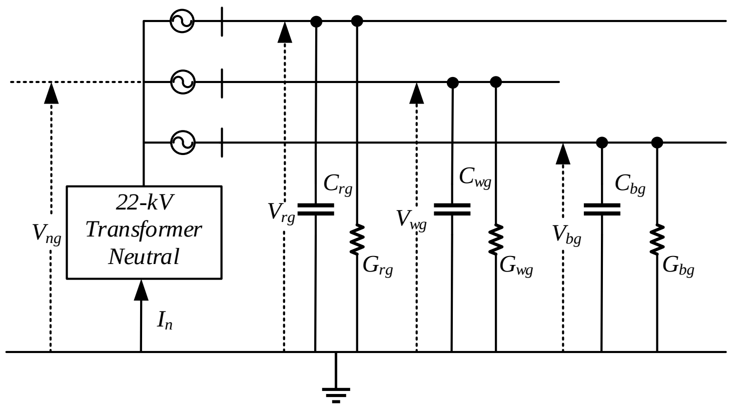

Fig. 5.1 Simplified representation of a 22-kV feeder

5.3 Capacitance of 22-kV feeder

Consider a 22-kV feeder. Fig. 5.2 shows one of the poles supporting the conductors of the feeder. Assuming we know the radius of conductors in the three 'rwb'-phases to be D_{rr}, D_{ww} and D_{bb}. Also, let us assume that we know the distances between the conductors as where $D_{rw} = D_{wr}, D_{wb} = D_{bw}$, and $D_{rb} = D_{br}$.

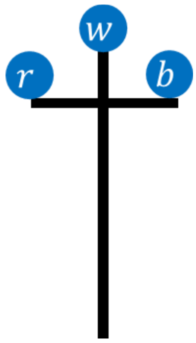

Fig. 5.2 Cross-sectional view of 'rwb' conductors in a pole supporting the 22-kV feeder

Given, q_r, q_w, and q_b charges flowing in the three phases, respectively, the charges will create independent electric fields. The charge q_r on conductor r generates a voltage V_{rw-r} between the rw phases. Similarly, the charge q_w on conductor w generates a voltage V_{rw-w} between the rw phases and the charge q_b on conductor b generates a voltage V_{rw-b} between the rw phases.

The voltage between the rw phases due to charge q_r can be calculated by integrating the electric field intensity [15, 16], E_r as follows:

$$V_{rw-r} = \int_{D_{rr}}^{D_{wr}} E_r dx = \int_{D_{rr}}^{D_{wr}} \frac{q_r}{2\pi\epsilon_0}\frac{dx}{x} = \frac{q_r}{2\pi\epsilon_0} ln\frac{D_{wr}}{D_{rr}} \tag{5.2}$$

where ϵ_0 is the permittivity of the free-space = 8.854×10^{-12}. Similarly, the voltage between the rw phases due to charge q_w can be calculated by integrating the electric field intensity, E_w as follows:

$$V_{rw-w} = \int_{D_{rw}}^{D_{ww}} E_w dx = \int_{D_{rw}}^{D_{ww}} \frac{q_w}{2\pi\epsilon_0}\frac{dx}{x} = \frac{q_w}{2\pi\epsilon_0} ln\frac{D_{ww}}{D_{rw}} \tag{5.3}$$

Finally, the voltage between the rw phases due to charge q_b can be calculated by integrating the electric field intensity, E_b as follows:

$$V_{rw-b} = \int_{D_{rb}}^{D_{wb}} E_b dx = \int_{D_{rb}}^{D_{wb}} \frac{q_b}{2\pi\epsilon_0}\frac{dx}{x} = \frac{q_b}{2\pi\epsilon_0} ln\frac{D_{wb}}{D_{rb}} \tag{5.4}$$

The total voltage is the sum of the generated voltages. Hence, we can obtain,

$$V_{rw} = V_{rw-r} + V_{rw-w} + V_{rw-b}$$
$$= \frac{1}{2\pi\epsilon_0}\left[q_r \ln\frac{D_{wr}}{D_{rr}} + q_w \ln\frac{D_{ww}}{D_{rw}} + q_b \ln\frac{D_{wb}}{D_{rb}}\right] \tag{5.5}$$

Similarly, the voltage between the two phases of three conductors in 'rwb' phases can be found as follows:

$$\begin{aligned} V_{rw} &= \frac{1}{2\pi\epsilon_0}\left[q_r \ln\frac{D_{wr}}{D_{rr}} + q_w \ln\frac{D_{ww}}{D_{rw}} + q_b \ln\frac{D_{wb}}{D_{rb}}\right] \\ V_{wb} &= \frac{1}{2\pi\epsilon_0}\left[q_r \ln\frac{D_{br}}{D_{wr}} + q_w \ln\frac{D_{bw}}{D_{ww}} + q_b \ln\frac{D_{bb}}{D_{wb}}\right] \\ V_{rb} &= \frac{1}{2\pi\epsilon_0}\left[q_r \ln\frac{D_{br}}{D_{rr}} + q_w \ln\frac{D_{bw}}{D_{rw}} + q_b \ln\frac{D_{bb}}{D_{rb}}\right] \end{aligned} \tag{5.6}$$

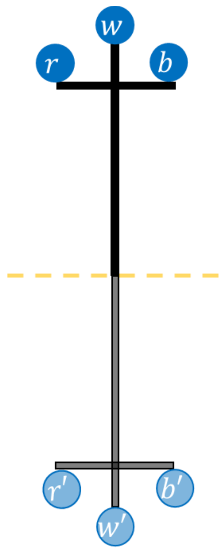

Fig. 5.3 Image '$r'w'b'$' conductors along with physical 'rwb' conductors in a pole supporting the 22-kV feeder

Since the return path of the 22-kV feeder is through the earth, we need to consider the effect of the earth. For this purpose, three image conductors r', w', and b' below the ground need to be considered. Fig. 5.3 shows the image conductors along with the physical conductors. The image conductors carry charges of $-q_r$, $-q_w$, and $-q_b$ respectively. The distances between a pair of image conductors are the same as the physical conductors that are above the ground, i.e., $D_{r'w'} = D_{w'r'} = D_{rw} = D_{wr}, D_{w'b'} = D_{b'w'} = D_{wb} = D_{bw}$, and $D_{r'b'} = D_{b'r'} = D_{rb} = D_{br}$. Also, let us consider the distances between the image conductors and the physical conductors $D_{rr'} = D_{r'r}, D_{ww'} = D_{w'w}, D_{bb'} = D_{b'b}, D_{rw'} = D_{w'r}, D_{rb'} = D_{b'r}, D_{wr'} = D_{r'w}, D_{wb'} = D_{b'w}, D_{br'} = D_{r'b}$, and $D_{bw'} = D_{w'b}$ are known. Now, considering the effect of image conductor, the previously developed voltage relations can be updated as follows:

$$\begin{aligned} V_{rw} = \frac{1}{2\pi\epsilon_0}\Big[& q_r \ln\frac{D_{wr}}{D_{rr}} + q_w \ln\frac{D_{ww}}{D_{rw}} + q_b \ln\frac{D_{wb}}{D_{rb}} - q_r \ln\frac{D_{wr'}}{D_{rr'}} \\ & - q_w \ln\frac{D_{ww'}}{D_{rw'}} - q_b \ln\frac{D_{wb'}}{D_{rb'}}\Big] \end{aligned} \tag{5.7}$$

Similarly, the voltage difference between positions r and r' can be obtained as follows:

$$V_{rr'} = \frac{1}{2\pi\epsilon_0}\left[q_r \ln\frac{D_{r'r}}{D_{rr}} + q_w \ln\frac{D_{r'w}}{D_{rw}} + q_b \ln\frac{D_{r'b}}{D_{rb}} + q_{r'} \ln\frac{D_{r'r'}}{D_{rr'}} + q_{w'} \ln\frac{D_{r'w'}}{D_{rw'}} + q_{b'} \ln\frac{D_{r'b'}}{D_{rb'}}\right] \tag{5.8}$$

which can be generalized as follows:

$$V_{kk'} = \frac{1}{2\pi\epsilon_0}\left[\sum_{m=\{r,w,b\}} q_m \ln\frac{D_{k'm}}{D_{km}} + \sum_{m=\{r',w',b'\}} q_m \ln\frac{D_{k'm}}{D_{km}}\right] \tag{5.9}$$

Since the image conductor charges are equal and opposite to the charges in the physical conductors, i.e., $q_{r'} = -q_r, q_{w'} = -q_w$, and $q_{r'} = -q_b$, the above relationship can be written as follows:

$$V_{kk'} = \frac{1}{2\pi\epsilon_0}\left[\sum_{m=\{r,w,b\}} q_m \ln\frac{D_{k'm}}{D_{km}} - \sum_{m=\{r',w',b'\}} q_m \ln\frac{D_{k'm}}{D_{km}}\right] \tag{5.10}$$

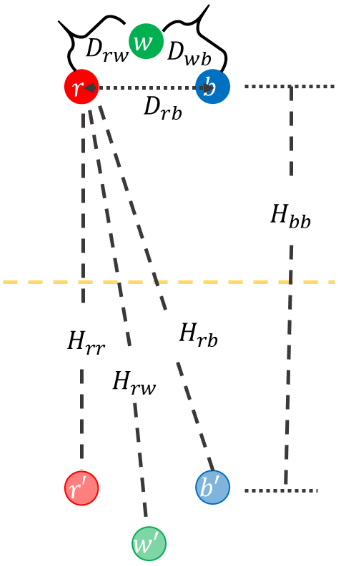

Fig. 5.4 Various distances in the physical and image conductor sets

For generalization, let us denote the distance between any physical conductor i and image conductor j as H_{ij}, as shown in Fig. 5.4. Hence, the above relationship can be represented as follows:

$$V_{kk'} = \frac{1}{2\pi\epsilon_0}\left[\sum_{m=\{r,w,b\}} q_m \ln\frac{H_{km}}{D_{km}} - \sum_{m=\{r',w',b'\}} q_m \ln\frac{D_{km}}{H_{km}}\right] \tag{5.11}$$

or,

$$V_{kk\prime} = \frac{1}{2\pi\epsilon_0}\left[\sum_{m=\{r,w,b,r',w',b\prime\}} q_m \, ln\left(\frac{H_{km}}{D_{km}}\right)^2\right] \tag{5.12}$$

or,

$$V_{kk\prime} = \frac{2}{2\pi\epsilon_0}\left[\sum_{m=\{r,w,b,r',w',b\prime\}} q_m \ln\frac{H_{km}}{D_{km}}\right] \tag{5.13}$$

or,

$$V_{kk\prime} = \frac{1}{\pi\epsilon_0}\left[\sum_{m=\{r,w,b,r',w',b\prime\}} q_m \ln\frac{H_{km}}{D_{km}}\right] \tag{5.14}$$

Now, because of symmetry the following relationship holds:

$$V_{kn} = \frac{1}{2}V_{kk\prime} = \frac{1}{2\pi\epsilon_0}\left[\sum_{m=\{r,w,b\}} q_m \ln\frac{H_{km}}{D_{km}}\right] \tag{5.15}$$

So, the phase-to-neutral voltages in the 22-kV network can be represented as follows:

$$\begin{aligned} V_{rn} &= \frac{1}{2\pi\epsilon_0}\left[q_r \, ln\frac{H_{rr}}{D_{rr}} + q_w \, ln\frac{H_{rw}}{D_{rw}} + q_b \, ln\frac{H_{rb}}{D_{rb}}\right] \\ V_{wn} &= \frac{1}{2\pi\epsilon_0}\left[q_r \, ln\frac{H_{wr}}{D_{wr}} + q_w \, ln\frac{H_{ww}}{D_{ww}} + q_b \, ln\frac{H_{wb}}{D_{wb}}\right] \\ V_{bn} &= \frac{1}{2\pi\epsilon_0}\left[q_r \, ln\frac{H_{br}}{D_{br}} + q_w \, ln\frac{H_{bw}}{D_{bw}} + q_b \, ln\frac{H_{bb}}{D_{bb}}\right] \end{aligned} \tag{5.16}$$

Now the following relationships holds among the charge, q_r, the impressed voltage, V_{rg}, due to the charge and formed capacitance, C_{rg}, due to the voltage:

$$C_{rg} = \frac{q_r}{V_{rg}} \tag{5.17}$$

or,

$$q_r = C_{rg}V_{rg} \tag{5.18}$$

Also, the voltage V_{rg} can be regarded as follows when we consider the neutral voltage:

$$V_{rg} = V_{rn} + V_{ng} \tag{5.19}$$

So, we obtain,

$$q_r = C_{rg}(V_{rn} + V_{ng}) \tag{5.20}$$

Similarly, for q_w and q_b we can obtain,

$$q_w = C_{wg}(V_{wn} + V_{ng}) \tag{5.21}$$

$$q_b = C_{bg}(V_{bn} + V_{ng}) \tag{5.22}$$

Replacing the charges in the previously developed voltage relations we can obtain,

$$\begin{aligned}
V_{rn} &= \frac{1}{2\pi\epsilon_0}\left[C_{rg}(V_{rn} + V_{ng})\, ln\frac{H_{rr}}{D_{rr}} + C_{wg}(V_{wn} + V_{ng})\, ln\frac{H_{rw}}{D_{rw}} \right. \\
&\qquad \left. + C_{bg}(V_{bn} + V_{ng})\, ln\frac{H_{rb}}{D_{rb}}\right] \\
V_{wn} &= \frac{1}{2\pi\epsilon_0}\left[C_{rg}(V_{rn} + V_{ng})\, ln\frac{H_{wr}}{D_{wr}} + C_{wg}(V_{wn} + V_{ng})\, ln\frac{H_{ww}}{D_{ww}} \right. \\
&\qquad \left. + C_{bg}(V_{bn} + V_{ng})\, ln\frac{H_{wb}}{D_{wb}}\right] \\
V_{bn} &= \frac{1}{2\pi\epsilon_0}\left[C_{rg}(V_{rn} + V_{ng})\, ln\frac{H_{br}}{D_{br}} + C_{wg}(V_{wn} + V_{ng})\, ln\frac{H_{bw}}{D_{bw}} \right. \\
&\qquad \left. + C_{bg}(V_{bn} + V_{ng})\, ln\frac{H_{bb}}{D_{bb}}\right]
\end{aligned} \tag{5.23}$$

which can be represented in matrix form as follows:

$$\begin{aligned}
&\begin{bmatrix} V_{rn} \\ V_{wn} \\ V_{bn} \end{bmatrix} \\
&= \frac{1}{2\pi\epsilon_0}\begin{bmatrix} (V_{rn} + V_{ng}) ln\frac{H_{rr}}{D_{rr}} & (V_{wn} + V_{ng}) ln\frac{H_{rw}}{D_{rw}} & (V_{bn} + V_{ng})\, ln\frac{H_{rb}}{D_{rb}} \\ (V_{rn} + V_{ng})\, ln\frac{H_{wr}}{D_{wr}} & (V_{wn} + V_{ng})\, ln\frac{H_{ww}}{D_{ww}} & (V_{bn} + V_{ng})\, ln\frac{H_{wb}}{D_{wb}} \\ (V_{rn} + V_{ng}) ln\frac{H_{br}}{D_{br}} & (V_{wn} + V_{ng})\, ln\frac{H_{br}}{D_{br}} & (V_{bn} + V_{ng})\, ln\frac{H_{bb}}{D_{bb}} \end{bmatrix}\begin{bmatrix} C_{rg} \\ C_{wg} \\ C_{bg} \end{bmatrix}
\end{aligned} \tag{5.24}$$

These relationships can be utilized to observe the effect of neutral voltage (V_{ng}) on the capacitance C_{rg}, C_{wg}, and C_{bg}.

Next, the relationship will be obtained when there is a mutual coupling between the 22-kV and the 66-kV feeder.

5.4 Capacitance of 22-kV feeder mutually coupled with 66-kV feeder

Now let us consider the effect of 66-kV lines that are above the 22-kV lines as shown in Fig. 5.5. The 66-kV lines are represented as ‘RWB’ conductors (top) and the 22-kV lines are represented as ‘rwb’ conductors. If we consider the coupling effect of three ‘RWB’ phases in the 66-kV feeder with the ‘rwb’ phases in the 22-kV feeder, we can extend the previous analysis to arrive at the voltage relationships in the ‘RWB’ and the ‘rwb’ phases.

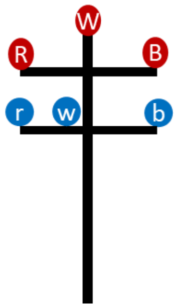

Fig. 5.5 Cross-sectional view of ‘rwb’ conductors in a pole supporting the 22-kV feeder (bottom) along with ‘RWB’ conductors of the 66-kV sub-transmission line

If the mutual effect of RWB phases is considered, the following matrix is found:

$$\begin{bmatrix} V_{Rn} \\ V_{Wn} \\ V_{Bn} \\ V_{rn} \\ V_{wn} \\ V_{bn} \end{bmatrix} = \frac{1}{2\pi\epsilon_0}\begin{bmatrix} (V_{RN}+V_{Ng})ln\frac{H_{RR}}{D_{RR}} & (V_{WN}+V_{Ng})ln\frac{H_{RW}}{D_{RW}} & (V_{BN}+V_{Ng})ln\frac{H_{RB}}{D_{RB}} & (V_{rn}+V_{ng})ln\frac{H_{Rr}}{D_{Rr}} & (V_{wn}+V_{ng})ln\frac{H_{Rw}}{D_{Rw}} & (V_{bn}+V_{ng})ln\frac{H_{Rb}}{D_{Rb}} \\ (V_{RN}+V_{Ng})ln\frac{H_{WR}}{D_{WR}} & (V_{WN}+V_{Ng})ln\frac{H_{WW}}{D_{WW}} & (V_{BN}+V_{Ng})ln\frac{H_{WB}}{D_{WB}} & (V_{rn}+V_{ng})ln\frac{H_{Wr}}{D_{Wr}} & (V_{wn}+V_{ng})ln\frac{H_{Ww}}{D_{Ww}} & (V_{bn}+V_{ng})ln\frac{H_{Wb}}{D_{Ww}} \\ (V_{RN}+V_{Ng})ln\frac{H_{BR}}{D_{BR}} & (V_{WN}+V_{Ng})ln\frac{H_{BW}}{D_{BW}} & (V_{BN}+V_{Ng})ln\frac{H_{BB}}{D_{BB}} & (V_{rn}+V_{ng})ln\frac{H_{Br}}{D_{Br}} & (V_{wn}+V_{ng})ln\frac{H_{Bw}}{D_{Bw}} & (V_{bn}+V_{ng})ln\frac{H_{Bb}}{D_{Bb}} \\ (V_{RN}+V_{Ng})ln\frac{H_{rR}}{D_{rR}} & (V_{WN}+V_{Ng})ln\frac{H_{rW}}{D_{rW}} & (V_{BN}+V_{Ng})ln\frac{H_{rB}}{D_{rB}} & (V_{rn}+V_{ng})ln\frac{H_{rr}}{D_{rr}} & (V_{wn}+V_{ng})ln\frac{H_{rw}}{D_{rw}} & (V_{bn}+V_{ng})ln\frac{H_{rb}}{D_{rb}} \\ (V_{RN}+V_{Ng})ln\frac{H_{wR}}{D_{wR}} & (V_{WN}+V_{Ng})ln\frac{H_{wW}}{D_{wW}} & (V_{BN}+V_{Ng})ln\frac{H_{wB}}{D_{wB}} & (V_{rn}+V_{ng})ln\frac{H_{wr}}{D_{wr}} & (V_{wn}+V_{ng})ln\frac{H_{ww}}{D_{ww}} & (V_{bn}+V_{ng})ln\frac{H_{wb}}{D_{wb}} \\ (V_{RN}+V_{Ng})ln\frac{H_{bR}}{D_{bR}} & (V_{WN}+V_{Ng})ln\frac{H_{bW}}{D_{bW}} & (V_{BN}+V_{Ng})ln\frac{H_{bB}}{D_{bB}} & (V_{rn}+V_{ng})ln\frac{H_{br}}{D_{br}} & (V_{wn}+V_{ng})ln\frac{H_{bw}}{D_{bw}} & (V_{bn}+V_{ng})ln\frac{H_{bb}}{D_{bb}} \end{bmatrix} \tag{5.25}$$

These relationships can be utilized to observe the effect of neutral voltage (V_{Ng}, V_{ng}) on the capacitance $C_{Rg}, C_{Wg}, C_{Bg}, C_{rg}, C_{wg}$, and C_{bg}.

5.5 Simulation results

The following unbalances can be calculated for a practical network with four different configurations as shown in Table 5.1. The phase voltages of the 22-kV network are $V_{rn} = 12701.70\ \text{kV}\angle 0°$, $V_{wn} = 12701.70\ \text{kV}\angle -120°$, and $V_{bn} = 12701.70\ \text{kV}\angle 120°$. The phase voltages of the 66-kV network are $V_{RN} = 38105.10 \text{ kV}\angle 0°$, $V_{WN} = 38105.10 \text{ kV}\angle -120°$, and $V_{BN} = 38105.10 \text{ kV}\angle 120°$.

The configuration 1 runs for 25.69 km with 'rwb' phasing of 22-kV line. In this configuration the conductors of the three phases are 7/.0104 SC-GZ with a radius of 3.9625 mm. The configuration 2 conductors are the same as configuration 1, with a 'brw' phasing that runs for 1.22 km. The length of lines in configuration 3 is 8.27 km with 'rwb' phasing. The conductor used in configuration 3 is 19/3.25AAC with a radius of 8.15 mm. The same conductors are used in the last configuration (configuration 4). The length of this configuration is 0.35 km.

Table 5.1 Calculation of unbalance current

Phase Voltages	Magnitude (V)	Angle (degree)
VRN	38105.10	0
VWN	38105.10	-120
VBN	38105.10	120
Vrn	12701.70	0
Vwn	12701.70	-120
Vbn	12701.70	120

		Configuration 1	Configuration 2	Configuration 3	Configuration 4	Feeder
	Phasing (22kV)	rwb	brw	rwb	brw	
	Conductor (22kV)	7/.0104 SC-GZ	7/.0104 SC-GZ	19/3.25AAC	19/3.25AAC	
	Phasing (66kV)	RWB	RWB	RWB	RWB	
	Conductor (66kV)	19/3.25AAC	19/3.25AAC	19/3.25AAC	19/3.25AAC	
	Length	25.692360	1.219060	8.265800	0.348600	35.525820
22kV	Capacitance (nF/km)	4.3695	4.3695	4.6462	4.6462	
		3.8707	3.8707	4.0466	4.0466	
		4.3695	4.3695	4.6462	4.6462	
	Imbalance (mA/km)	1.9905	1.9905	2.3926	2.3926	
	Imbalance (degree)	-30.0000	90.0000	-30.0000	90.0000	
	Configuration Imbalance (mA)	51.1399	2.4265	19.7770	0.8341	
	Configuration Imbalance (degree)	-30.0000	90.0000	-30.0000	90.0000	
	Feeder Imbalance (mA)					69.3442
	Feeder Imbalance (degree)					-27.6662
22kV+66kV	Capacitance	-2.5926	-2.5926	-2.7611	-2.7611	
		-3.9660	-3.9660	-4.3167	-4.3167	
		-2.5926	-2.5926	-2.7611	-2.7611	
	Imbalance (mA/km)	5.4804	5.4804	6.2073	6.2073	
	Imbalance (degree)	-30.0000	90.0000	-30.0000	90.0000	
	Configuration Imbalance (mA)	140.8043	6.6809	51.3086	2.1639	
	Configuration Imbalance (degree)	-30.0000	90.0000	-30.0000	90.0000	
	Feeder Imbalance (mA)					187.8468
	Feeder Imbalance (degree)					-27.6630
	Difference of Imbalance (mA)					118.5062
	Difference of Imbalance (mA)					-27.6611

The capacitances are calculated for each configuration and the imbalance current (mA/km) is obtained by multiplying the capacitances with respective voltages. This imbalance multiplied by the total configuration length gives the configuration imbalance (mA). Summing up all imbalances gives total feeder imbalance (mA). This calculation is done for 22-kV lines alone and for the feeder where 22-kV and 66-kV lines share poles. From this calculation it can be summarized that:

- The imbalance is impacted by the addition of 66-kV, addition of 66-kV network alters the 22-kV line to neutral capacitances and hence the imbalance is changed,
- The imbalances in different phases are different because of the layout of cables on the poles,
- The configuration imbalance angle depends on the phasing, e.g., in configuration 1, the middle phase is ‘w’ with voltage angle $\angle -120°$ which corresponds to capacitive current angle of $\angle -30°$. Similarly, for ‘brw’ phasing the imbalance angle is $\angle 90°$ which corresponds to the middle phase voltage angle of ‘r’ phase.

Now the following cases are analysed.

5.5.1 Impact of change of neutral voltage magnitude in 22kV system

With $V_{rn} = V_{wn} = V_{bn} = 12701.7V$, the feeder imbalance is found to be $69.34mA\angle -27.67°$ in 22-kV system when the neutral voltage is zero. In practical, the imbalance is minimized by adding extra capacitors in different phases based on the imbalance. To mimic this, we injected some capacitance in phase w that makes the imbalance $33.53mA\angle -25.27°$. The objective was to make the imbalance less than 50mA.

Similarly for the coupled 22-kV and the 66-kV system, the feeder imbalance is found to be $187.83mA\angle -27.65°$ when the neutral voltage is zero, $V_{rn} = V_{wn} = V_{bn} = 12701.7V$, and $V_{RN} = V_{WN} = V_{BN} = 38105.1V$. Here some capacitances are injected in phase w to make the imbalance go down to $44.69mA\angle -20.08°$.

In case of a fault, the neutral voltage rises very high around the rated phase voltage also GFN rises the voltage for bushfire mitigation purposes. Also, during the RCC fault confirmation process, the neutral voltage is varied 85% to 100% of the rated voltage. To consider this situation the neutral voltage magnitude is varied between 10kV to 12.7kV and the change of admittance is observed. In the first case, the angle of the neutral voltage is considered 0°. The result is shown in Fig. 5.6(a) for the 22-kV system, in Fig. 5.6(b) for the coupled 22-kV and 66-kV system and in Fig. 5.6(c) for the coupled 22-kV and 66-kV system where the 66-kV network is not energised.

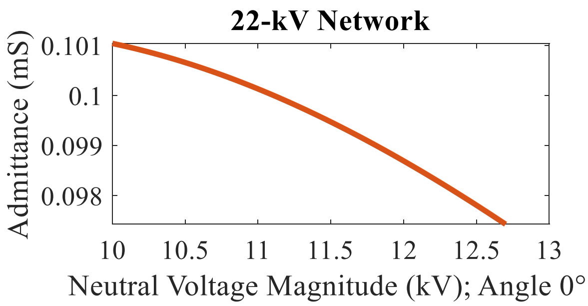

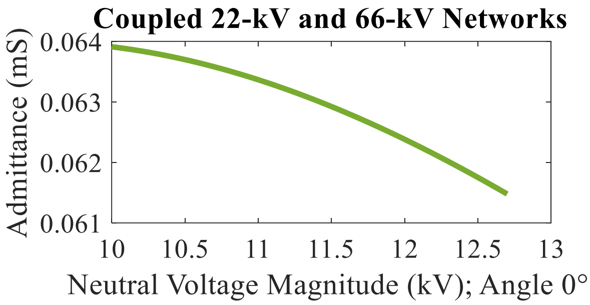

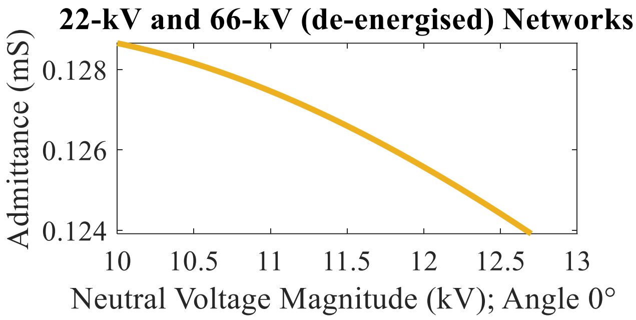

Fig. 5.6 Change in admittance with neutral voltage magnitude change, (a) 22-kV network, (b) coupled 22-kV and 66-kV network (c) coupled 22-kV and 66-kV network with 66-kV lines de-energised

It can be observed that the admittance changes from 0.1010mS to 0.0094mS as the neutral voltage magnitude is altered from 10kV to 12.7kV, resulting in a difference of 0.0036mS in the 22-kV network. For the 22-kV network that shares the 66-kV lines, the change of admittance is 0.0024mS. This change is from 0.0639mS for 10kV neutral voltage to 0.0615mS for 12.7kV neutral voltage. The admittance is the highest when the 22-kV network is coupled with the de-energised 66-kV network. Here the admittance is changed from 0.1287mS to 0.1239mS (with a 0.0048mS admittance change) when the neutral voltage magnitude is varied between 10kV to 12.7kV.

5.5.2 Impact of change of neutral voltage angle in 22kV system

The neutral voltage of the 22-kV network is varied between 10kV and 12.7kV for different neutral voltage angles and represented in Table 5.2.

Table 5.2 Change of admittance in mS in the 22-kV and the coupled 22-kV & 66-kV networks with change of 22-kV neutral voltage magnitude

Angle (degree)	22-kV Network			22-kV and 66-kV Network		
	10kV	12.7kV	Difference	10kV	12.7kV	Difference
0	0.1010	0.0974	-0.0036	0.0639	0.0615	-0.0024
30	0.0934	0.0968	0.0034	0.0602	0.0646	0.0044
60	0.0475	0.0416	-0.0059	0.0092	0.0070	-0.0022
90	0.0936	0.0969	0.0033	0.0595	0.0642	0.0047
120	0.1013	0.0976	-0.0037	0.0632	0.0611	-0.0021
150	0.0937	0.0981	0.0045	0.0566	0.0587	0.0021
180	0.0405	0.0359	-0.0046	0.0213	0.0171	-0.0041

From Table 5.2, it is observed that the admittance decreases with the increase of neutral voltage for some angles. The angles where the admittance deceases with the increase of neutral voltage are $0°, 60°, 120°,$ and $180°$. However, the admittance increases with the increase of neutral voltage where the angles are $30°, 90°,$ and $150°$. Since an effect of angle on the admittance change is observed, the impact of neutral voltage angle is investigated further.

During the fault confirmation process the angles are varied in the neutral by keeping the magnitude constant. So, in this case, the neutral voltage magnitude is kept at the rated value of 22-kV while the angle is varied between 0° to 360° and the result is shown in Fig 5.7.

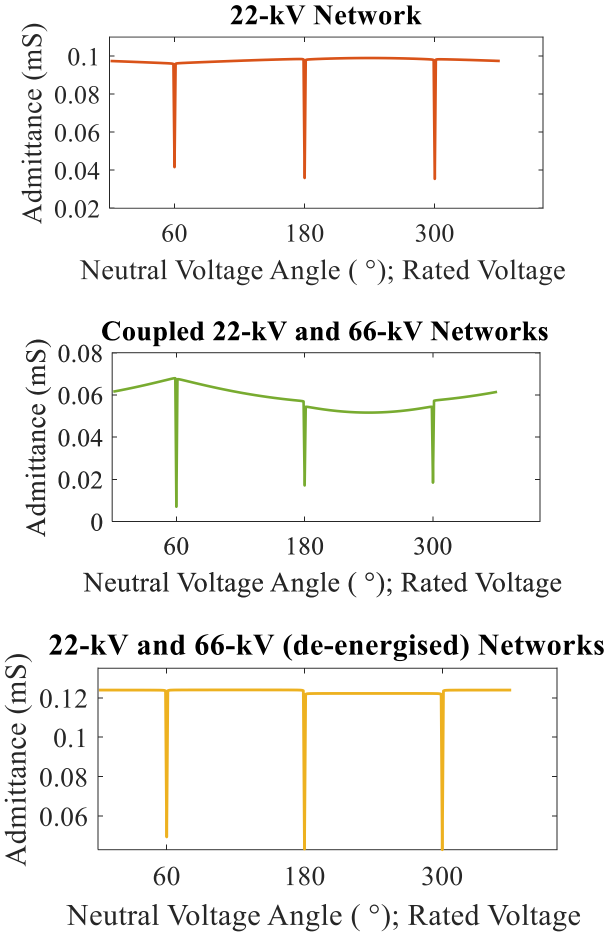

Fig. 5.7 Change in admittance with neutral voltage angle when rated voltage is applied at the neutral, (a) 22-kV network (b) coupled 22-kV and 66-kV network (c) coupled 22-kV and 66-kV network with 66-kV lines de-energised

A sudden jump in admittance is observed at $60°, 180°,$ and $300°$ where the neutral voltage angles correspond to the phase voltage angles. For example, the angle of r phase is the reference angle, which is 0°. Since a voltage out-of-phase with the phase voltages is applied at the neutral the neutral voltage angle corresponding to phase r is (0+180)° = 180°. Similarly, the neutral voltage angle corresponding to phase w is (-120+180)° = 60° and that to phase b is (120+180)° = 300°. It is observed that the admittance of the network jumps abruptly at these corresponding angles of the neutral voltage for both the 22-kV and the coupled network as shown in Fig 5.7. The change of admittance is also observed in Table 5.3 where the specific admittance values are found.

Table 5.3 Admittance in mS in the 22-kV and the coupled 22-kV & 66-kV networks with change of 22-kV neutral voltage angle

	Rated Voltage		85% of Rated Voltage	
Angle (degree)	22-kV	22- & 66-kV	22-kV	22- & 66-kV
1	0.09741	0.06157	0.10035	0.06359
59	0.09584	0.06793	0.04623	0.01054
60	0.04161	0.00700	0.04563	0.00853
61	0.09596	0.06747	0.04627	0.01009
179	0.09823	0.05693	0.03997	0.02089
180	0.03592	0.01710	0.03908	0.01992
181	0.09793	0.05438	0.03981	0.02002
299	0.09792	0.05438	0.03928	0.02148
300	0.03543	0.01844	0.03852	0.02147
301	0.09810	0.05724	0.03940	0.02243
360	0.09743	0.06148	0.10036	0.06352

During the fault confirmation process, the neutral voltage is changed to some percentage of the rated value. Here a rated 85% of voltage is applied at the 22-kV neutral and the angles are varied. Similar to the previous analysis the admittance reaches a local minimum at 30°, 180°, and 300° as shown in Fig. 5.8. However, this change is not as steep as in Fig. 5.7 and left part of Table 5.3, rather the change is gradual over a certain angle range. Moreover, local maxima are also found within the ranges. For example, there is a local maximum between angles 60° and 180°; 180° and 300°; as well as 300° and 60°. Finally, the dynamic range of admittance in these ranges also vary.

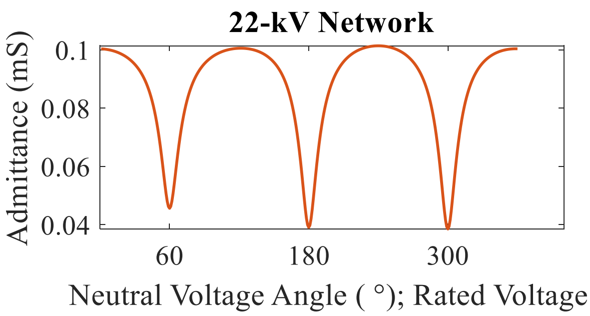

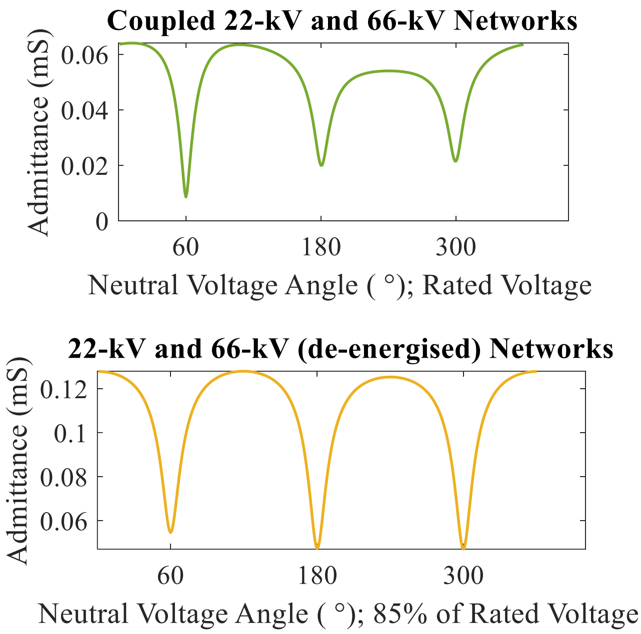

Fig. 5.8 Change in admittance with neutral voltage angle when 85% of rated voltage is applied at the neutral, (a) 22-kV network (b) coupled 22-kV and 66-kV network (c) coupled 22-kV and 66-kV network with 66-kV lines de-energised

From the analysis it can summarised that,

- If the neutral voltage angle is different, change is same neutral voltage magnitude will incur different changes in admittance,

- When the rated voltage is applied in neutral, the admittance change for neutral angle change is not very significant when the 22-kV system is considered alone. However, when the 66-kV system is coupled with the 22-kV system, some admittance change are noticed with neutral voltage angle change.

5.5.3 Impact of change of phase voltage magnitude in 66kV system

Next the impact of change of phase voltage in the 66-kV network is observed. Here the 66-kV phase voltage is varied from 0V to the rated voltage with the neutral voltage of 22-kV as 30V∠0° and the neutral voltage of 66-kV as 0V∠0°. The observed results are shown in Fig. 5.9. Hence it can be summarised that,

- linear change in imbalance magnitude is observed.

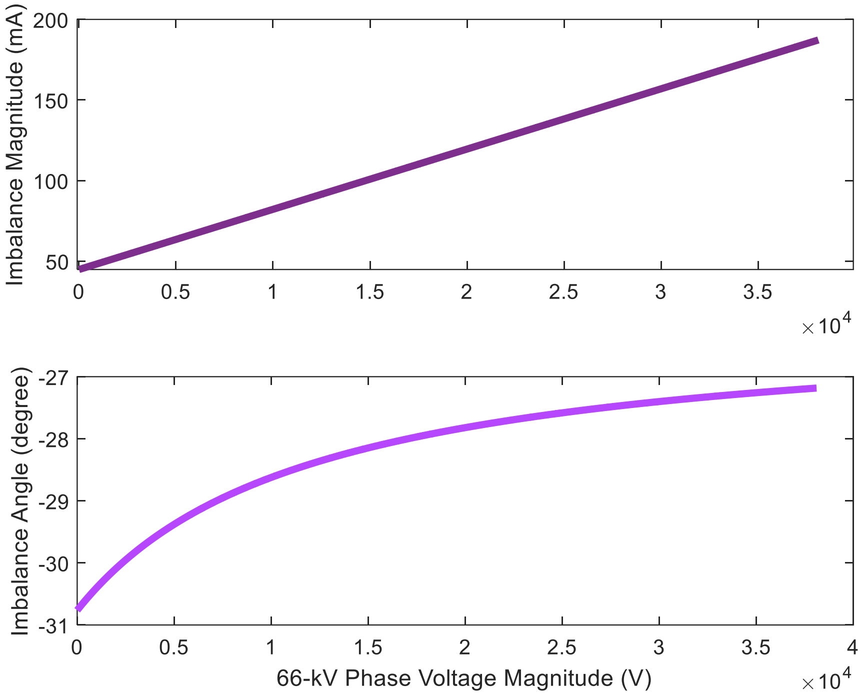

Fig. 5.9 Change in imbalance in the 22-kV network when the coupled 66-kV network phase voltage is varied

5.5.4 Impact of change of neutral voltage magnitude and angle in 66kV system

In order to observe the effect of neutral voltage in 66-kV network on the imbalance of the 22-kV network a) the magnitude of the neutral voltage in 66-kV network is varied by keeping the angle fixed (0°) and b) the neutral voltage angle in the 66-kV network is varied by keeping the magnitude fixed (1000V). The effects are observed in Fig. 5.10 and Fig. 5.11, respectively. It can be summarised that

- the neutral voltage of 66-kV doesn’t have any impact on the imbalance.

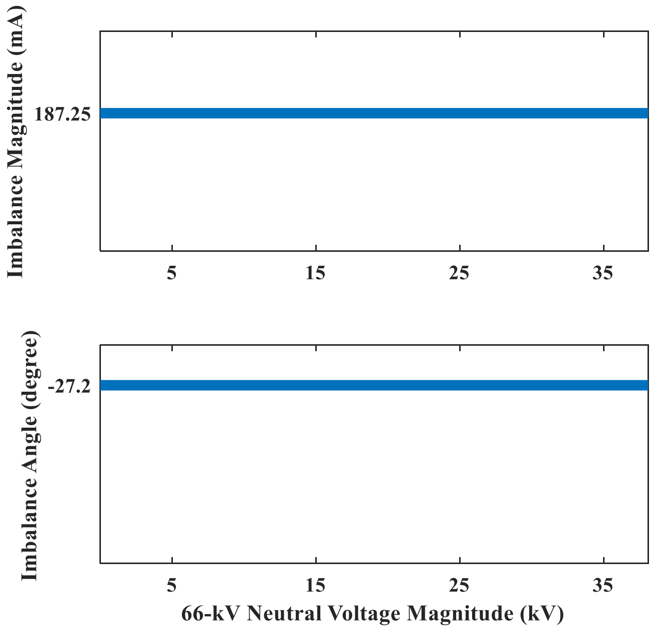

Fig. 5.10 Imbalance in 22-kV network versus 66-kV neutral voltage magnitude

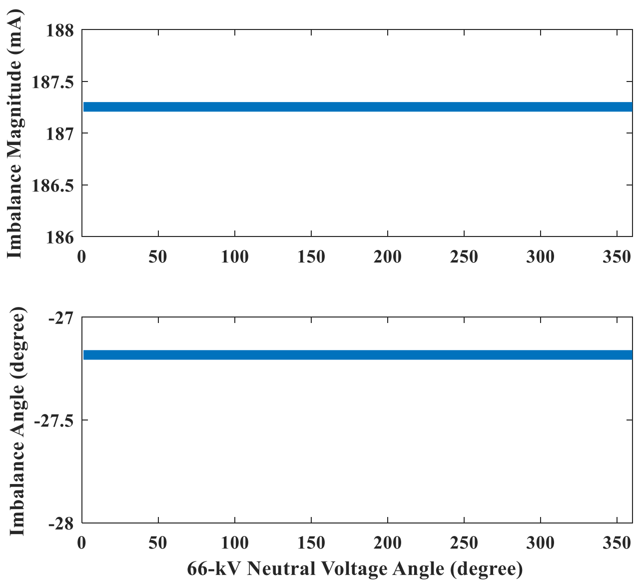

Fig. 5.11 Imbalance in 22-kV network versus 66-kV neutral voltage angle

5.5.5 Impact of transposing the 22kV system

Now to explore the impact of transposition in the 22-kV network on the mutually coupled system the Configuration 1 that runs for 25.69km is transposed. In this way, three cases are obtained. The first case is the same as Configuration 1 and the phasing in the 22-kV system is rwb and that of the 66-kV system is RWB. The phasing of RWB is kept constant while the 22-kV phasing is transposed. The phasing is brw in the second case and wbr in the third case. The resultant imbalance in the considered cases are $140.81\text{mA}\angle -30°$, $140.81\text{mA}\angle 90°$, and $140.81\text{mA}\angle -150°$ respectively. As a result, the imbalances are balanced out. However, when the phasing of the 66-kV is altered by keeping the phasing of 22-kV same, the imbalance doesn't balance out. The results are summarised in Table 5.4. Hence, it can be summarised that,

- transposition of 22-kV system might balance out the system considering other factors are similar. Hence phase transpose might reduce imbalance.

Table 5.4 Impact of transposition

	Network		Imbalance	
	22kV	22+66kV	Magnitude (mA)	Angle (degree)
Phasing	rwb	RWB	140.81	-30
Phasing	brw	RWB	140.81	90
Phasing	wbr	RWB	140.81	-150
Phasing	rwb	RWB	140.81	-30
Phasing	rwb	BRW	140.81	-30
Phasing	rwb	WBR	140.81	-30

5.5.6 Impact of change in cable size

In the next analysis, the cable size is changed, and result is shown in Table 5.5. It can be observed that

- the imbalance increases in magnitude with the increased radius of the cables.

Table 5.5 Impact of change in cable size

Network				Imbalance	
22-kV	Radius	66-kV	Radius	(mA/km)	degree
7/.0104 SC-GZ	3.9625	7/.0104 SC-GZ	3.9625	5.251315292	-30
7/.0104 SC-GZ	3.9625	19/3.25AAC	8.15	5.480395602	-30
19/3.25AAC	8.15	7/.0104 SC-GZ	3.9625	5.953186529	-30
19/3.25AAC	8.15	19/3.25AAC	8.15	6.207340273	-30
	2		2	4.549623795	-30
	11		11	6.693532741	-30

5.5.7 Impact of length change in 22kV system

Furthermore, the effect of change of length was observed. The length of all configurations were changed to 30% and 70% of the original length. This change of length changes the imbalance proportionally and hence the admittance change is also proportional to the length change. The results are shown in Fig. 5.12 for the 22-kV system and in Fig. 5.13 for the coupled 22- and 66-kV system. In all cases, the summary of the observation is as follows:

- effect on admittance is proportional to the length change.

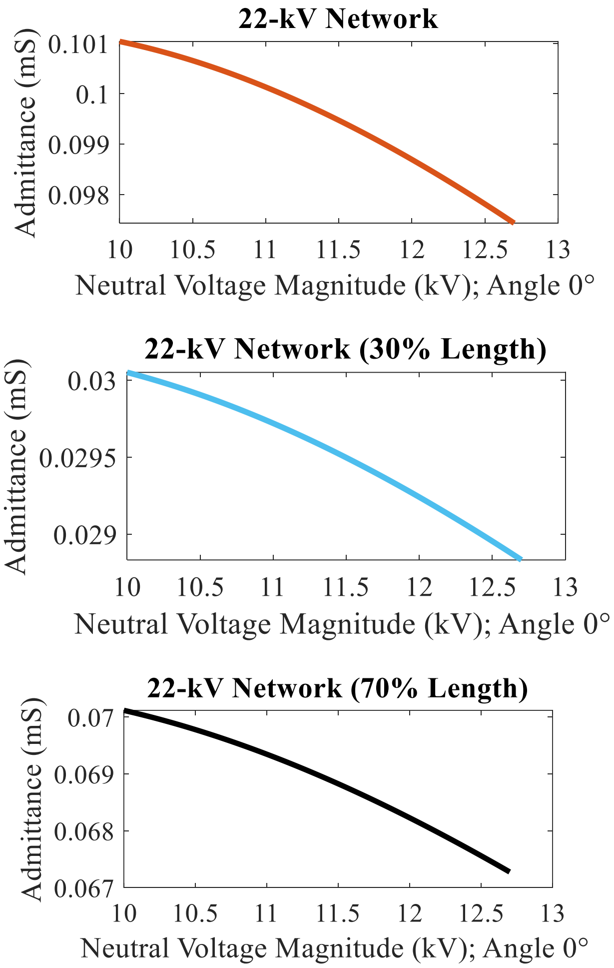

Fig. 5.12 Admittance in 22-kV network when the configuration length is (a) original (b) 30% of original and (c) 70% of original

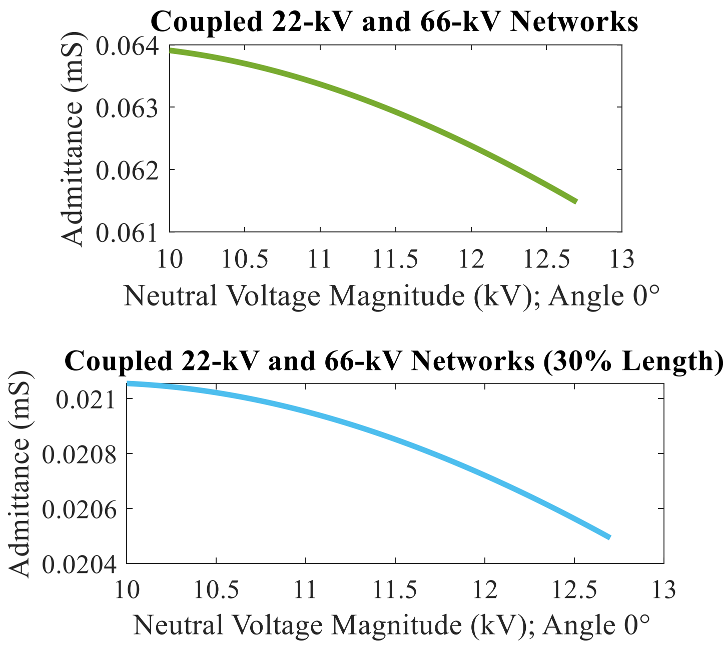

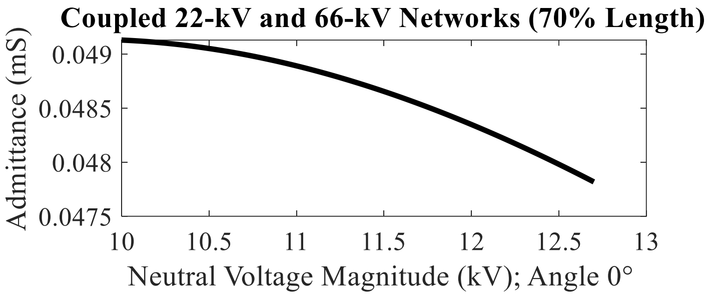

Fig. 5.13 Admittance in coupled 22- and 66-kV network when the configuration length is (a) original (b) 30% of original and (c) 70% of original

5.5.8 Impact of shifting the imbalance corresponding to different phases

In the previous analysis, the imbalance angle was close to -30°, which is close to the capacitive current angle (-120° + 90° = -30° in phase 'w'. Next, the network imbalance is shifted towards other phases, i.e., phases 'r' and 'b'. Three initial imbalance cases were observed. In case 1, the imbalance was made $30.41\text{mA}\angle 87.57°$, close to phase 'r'. Similarly, case 2 was close to phase 'w' with imbalance of $33.53\text{mA}\angle 25.27°$ and case 3 was close to phase 'b' with imbalance $29.62\text{mA}\angle -152.85°$. For all these cases the admittance change in the 22-kV network was observed when the 22-kV neutral voltage was varied. The result of admittance changes with the neutral voltage angle change as rated voltage is applied at the neutral, as shown in Fig. 5.14. The same simulation is carried out in Fig. 5.15 for the case when the neutral voltage magnitude is reduced to 85% of the rated voltage.

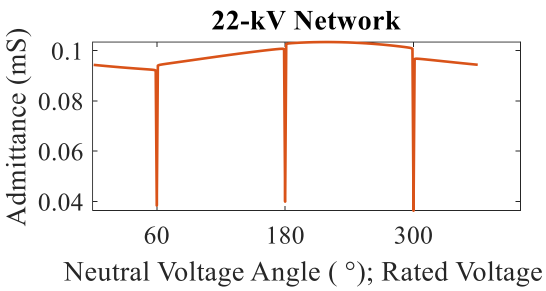

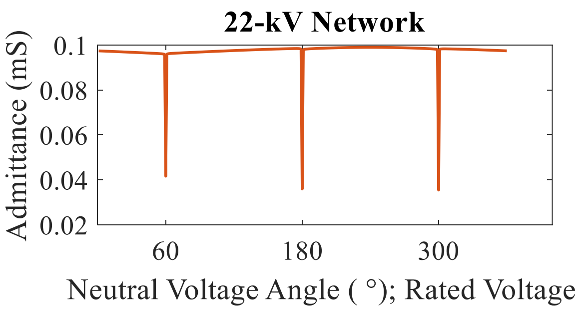

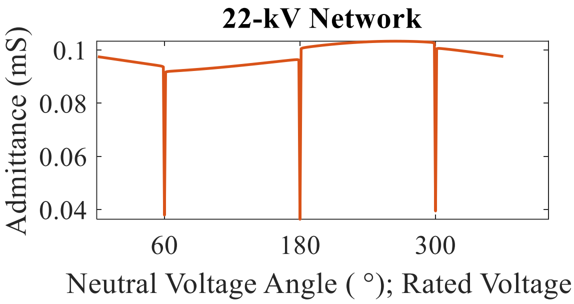

Fig. 5.14 Change of Admittance with 22-kV Neutral Voltage Angle Change and the rated magnitude (a) Imbalance 30.41mA angle 87.57 degrees (b) Imbalance 33.53mA angle -25.27 degrees (c) Imbalance 29.62mA angle -152.85 degrees

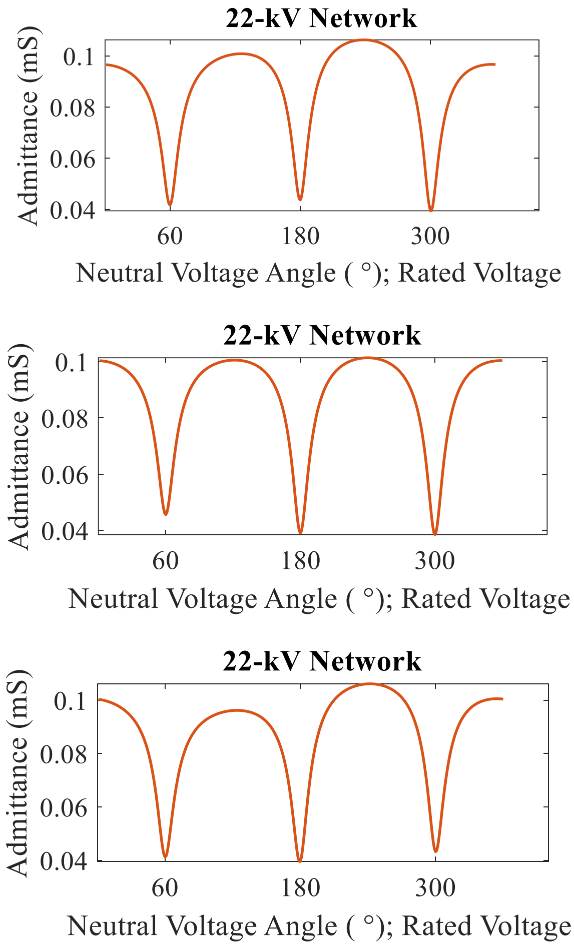

Fig. 5.15 Change of Admittance with 22-kV Neutral Voltage Angle Change and the 85% of rated magnitude (a) Imbalance 30.41mA angle 87.57 degrees (b) Imbalance 33.53mA angle -25.27 degrees (c) Imbalance 29.62mA angle -152.85 degrees

The results in Fig. 5.14 and Fig. 5.15 are repeated for the coupled system and shown in Fig. 5.16 and Fig. 5.17 respectively. From the results no noticeable pattern was observed when the initial imbalance was changed except for the case when the imbalance angle was close to ‘w’. Hence, this change can be attributed due to the asymmetry of configuration around phase ‘w’ but not due to initial imbalance.

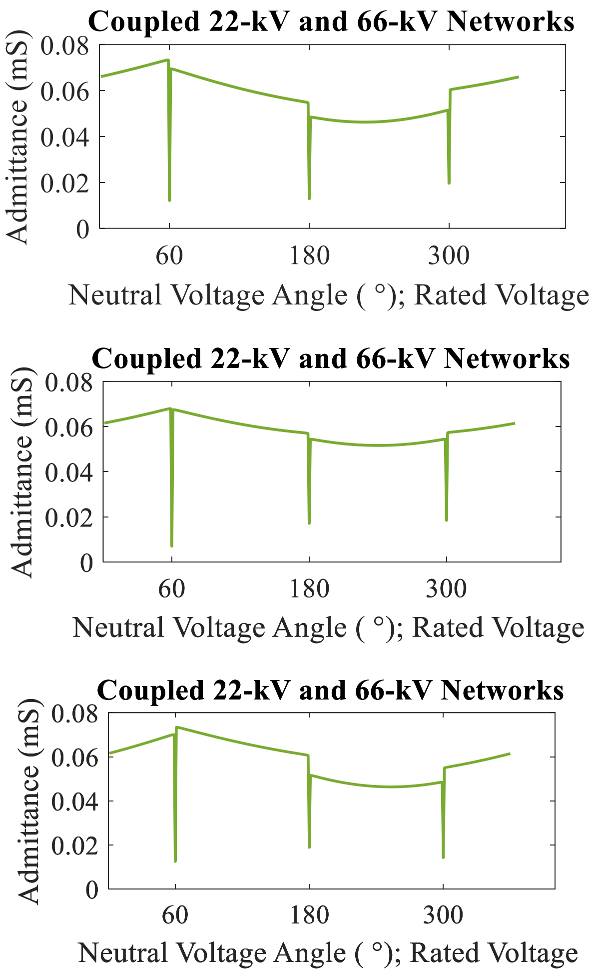

Fig. 5.16 Change of Admittance in the coupled network with 22-kV Neutral Voltage Angle Change and the rated magnitude (a) Imbalance close to red phase (b) Imbalance close to white phase (c) Imbalance close too blue phase

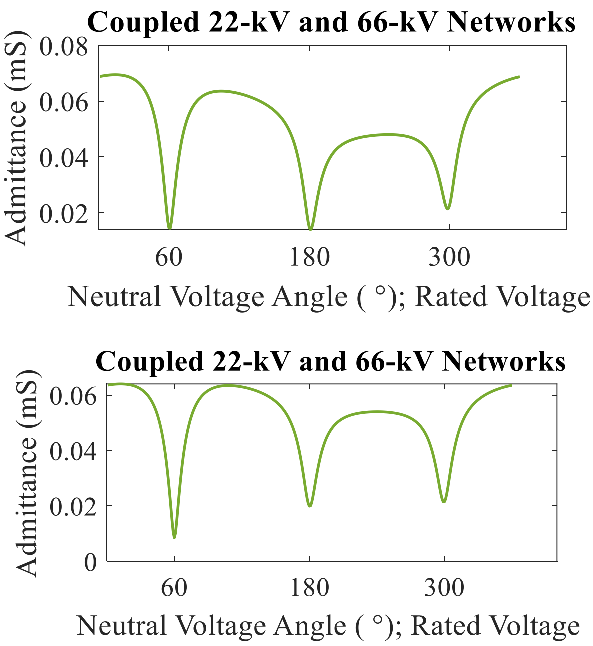

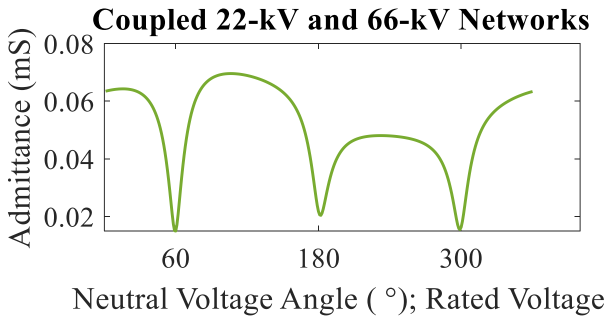

Fig. 5.17 Change of Admittance in the coupled network with 22-kV Neutral Voltage Angle Change and the 85% rated magnitude (a) Imbalance close to red phase (b) Imbalance close to white phase (c) Imbalance close too blue phase

Here, no specific trend has been observed and can be concluded that this parameter has no observable impact.

5.5.9 Impact of damping

In the analysis of impact of damping, shunt capacitances are neglected. Table 5.6 shows the estimated shunt resistances in different AusNet networks. The neutral voltage magnitude is kept at 85% of the rated value while the angle is varied between 0 and 360 degrees. This will in effect change the phase to ground voltages in the 22-kV and the resulting neutral current will change. As a result, the admittance will also change. The change of admittance is observed in Fig. 5.18. The admittance change depends on the existing imbalance in damping in three phases.

Table 5.6 Estimated damping in different AusNet networks

	Resistive losses (G)		
Feeders	r (mA)	w (mA)	b (mA)
SMR14	444	424	532
WN3	419	480	501
WN5	491	440	467
WN6	269	289	299
RUBA12	335	306	370
WYK12	206	204	206
WYK13	1609	1635	1596
WYK24	1355	1355	1381
MSD1	273	249	279

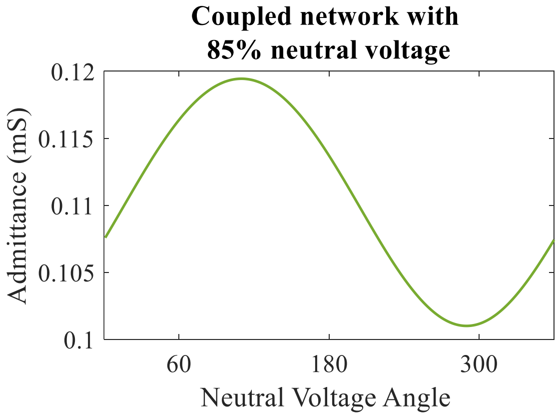
Coupled network with
85% neutral voltage
Admittance (mS)
0.12
0.115
0.11
0.105
0.1
60
180
300
Neutral Voltage Angle

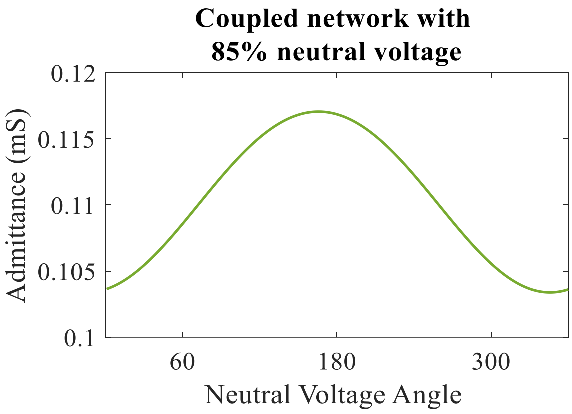
Coupled network with
85% neutral voltage
Admittance (mS)
0.12
0.115
0.11
0.105
0.1
60
180
300
Neutral Voltage Angle

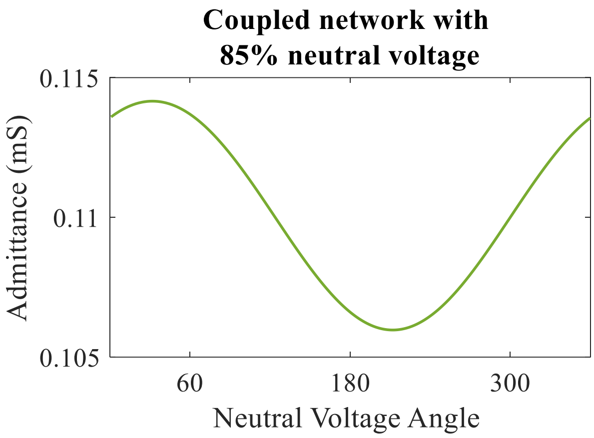
Coupled network with
85% neutral voltage
Admittance (mS)
0.115
0.11
0.105
60
180
300
Neutral Voltage Angle

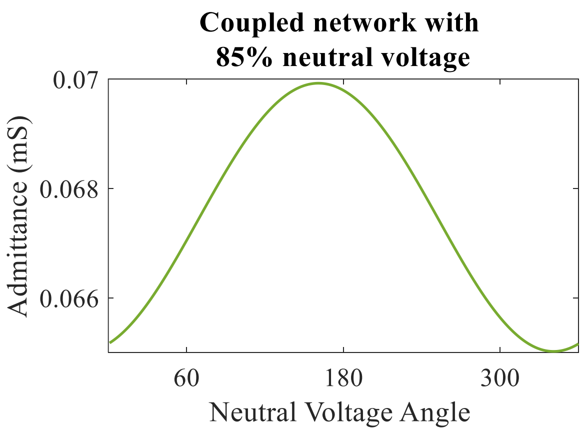
Coupled network with
85% neutral voltage
Admittance (mS)
0.07
0.068
0.066
60
180
300
Neutral Voltage Angle

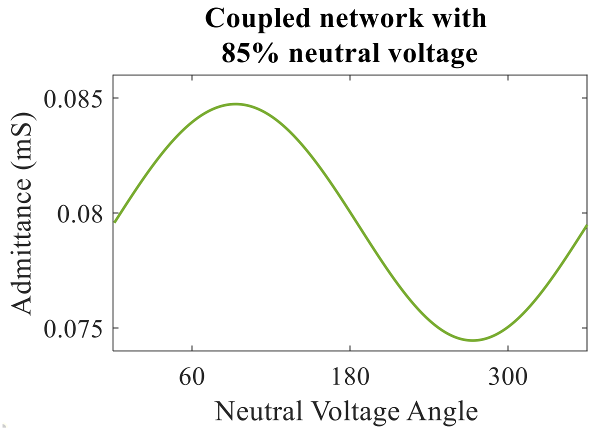
Coupled network with
85% neutral voltage
0.085
0.08
0.075
Admittance (mS)
60
180
300
Neutral Voltage Angle

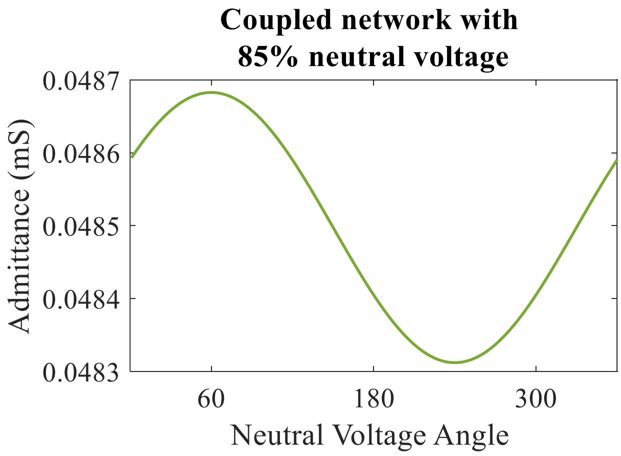
Coupled network with
85% neutral voltage
0.0487
0.0486
0.0485
0.0484
0.0483
Admittance (mS)
60
180
300
Neutral Voltage Angle

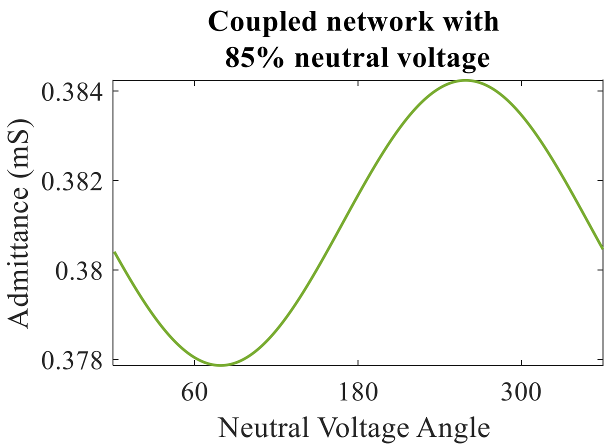
Coupled network with
85% neutral voltage
0.384
0.382
0.38
0.378
Admittance (mS)
60
180
300
Neutral Voltage Angle

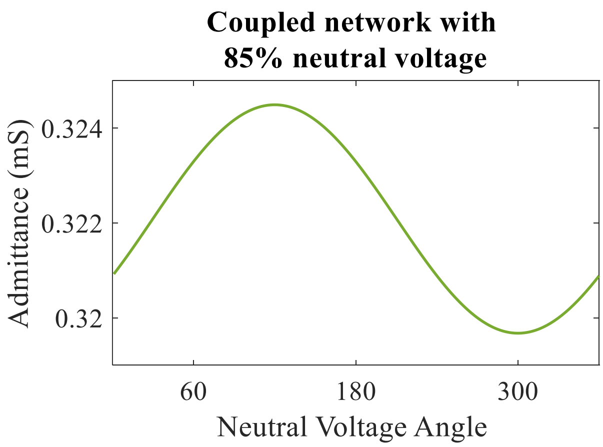
Coupled network with
85% neutral voltage
0.324
0.322
0.32
Admittance (mS)
60
180
300
Neutral Voltage Angle

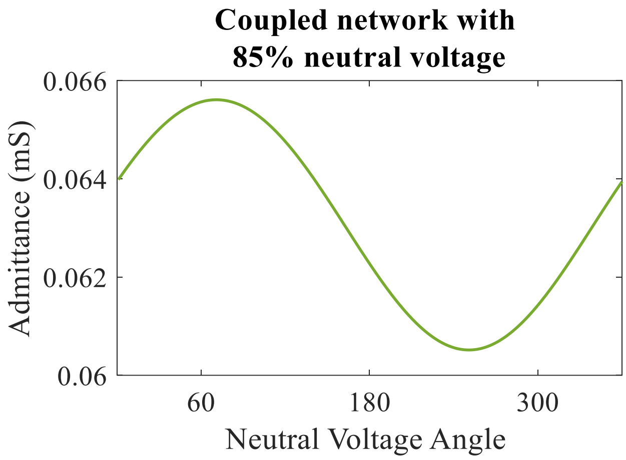

Fig. 5.18 Effect of damping in the admittance of the coupled network with 22-kV Neutral Voltage Angle Change and the 85% rated magnitude in different AusNet networks (a) SMR14 (b) WN3 (c) WN5 (d) WN6 (e) RUBA12 (f) WYK12 (g) WYK13 (h) WYK24 (i) MSD1

Moreover, a faulted condition in the network is simulated and the change in admittance related to the corresponding faulted phases are investigated. The admittance values are given in Table 5.7. Here the angle is changed from 180 degree to 210 degree for 'r' phase, from 60 degree to 90 degree for 'w' phase and from 300 degree to 330 degree for 'b' phase. The resulting change in admittance is observed in Table 5.7. It is to again note that capacitance are neglected.

Table 5.7 Change of admittance in faulted condition due to damping

	Faulted (25.4kΩ) phase		
Feeders	r	w	b
SMR14	31.41	-32.27	44.39
WN3	37.03	-34.70	37.11
WN5	39.36	-41.06	43.97
WN6	57.02	-56.71	58.22
RUBA12	47.23	-48.03	56.68
WYK12	71.27	-71.26	71.59
WYK13	6.87	-5.95	3.97
WYK24	7.97	-7.97	9.40
MSD1	59.50	-59.78	64.27

Hence it can be summarized that,

- The delta admittance errors depend on the existing imbalance in resistive losses among different phases,
- The delta admittance errors also depend on the system fault conditions,
- For a non-faulted system with balanced resistive losses, the delta admittance errors are negligible.

5.6 Discussion on objectives, deliverables and intended outcomes

A mathematical model has been developed that effectively analyses the impact of 66kV lines on the unbalance of 22kV lines. The impact of various parameters on the neutral current of 22kV line has been analysed. If the resonant grounded system is operating in steady state, i.e., the system has no fault then the impact of coupling in neutral current is negligible. The deviation of the neutral current depends on the system fault condition.

5.7 Future outlook

The present analysis has been carried out for a single feeder in AusNet services that share 22kV and 66kV lines is same poles for a considerable distance. The analysis can be validated with results from different networks in future.

Chapter 6
Summary of the Project

6.1 Introduction

The aim of the project named "Performance Analysis of Compensated Distribution Networks in Bushfire Prone Areas" is to provide a performance assessment to investigate the potential impacts of implementing Rapid Earth Fault Limiter (REFCL) technology on selected AusNet Services rural networks. This project has fulfilled the research scopes by completing the prescribed four tasks. The deliverable outputs have been achieved which are as follows:

(i) An algorithm for estimating the fault location and the voltage at the fault location.
(ii) A ranking of different factors affecting the voltage at the fault location.
(iii) An adaptive scheme for calculating the network damping using real-time information.
(iv) A framework for analysing the impacts of sub-transmission lines on the network imbalance of distribution lines.

6.2 Future outlook

It is expected that the investigated mechanisms employed in the final reports will help to improve the performance of the compensated distribution network. The proposed algorithm of identification of fault location and estimation of voltage at fault location not only assists to reduce the faulty phase voltage for minimising bushfire risk but also reduce the duration of power outage. The sensitivity analysis of different factors affecting the voltage at the fault location helps to reduce the voltage at fault location and to maintain the thermal energy within the limit. In this way, this assists the distribution network service providers to concentrate on factors that severely affect the phase voltage at the fault location and to take appropriate steps to mitigate the adverse effects of powerline bushfires. Machine learning based gain tuning approaches can be considered to change the gain of the designed adaptive controller that can adjust the gain depending on the current dynamic range of the operating condition. This approach would provide better accuracy and reduce estimation errors significantly.

6.3 Conclusion

All deliverables related to the project have been achieved. The obtained deliverable outcomes of the project will help to improve the performance of compensated distribution networks.

References

[1] S. Lee *et al.*, “An intelligent and efficient fault location and diagnosis scheme for radial distribution systems,” *IEEE Trans. Power Del.*, vol. 19, no. 2, pp. 524-532, Apr. 2004.

[2] K. Sun, Q. Chen, and Z. Gao, “An automatic faulted line section location method for electric power distribution systems based on multisource information,” *IEEE Trans. Power Del.*, vol. 31, no. 4, pp. 1542-1551, Aug. 2016.

[3] D. Spoor and J. G. Zhu, “Improved single-ended traveling-wave fault-location algorithm based on experience with conventional substation transducers,” *IEEE Trans. Power Del.*, vol. 21, no. 3, pp. 1714-1720, Jul. 2006.

[4] R. H. Salim, K. R. C. de Oliveira, A. D. Filomena, M. Resener, and A. S. Bretas, “Hybrid fault diagnosis scheme implementation for power distribution systems automation,” *IEEE Trans. Power Del.*, vol. 23, no. 4, pp. 1846-1856, Oct. 2008.

[5] D. Thukaram, H. P. Khincha, and H. P. Vijaynarasimha, “Artificial neural network and support vector Machine approach for locating faults in radial distribution systems,” *IEEE Trans. Power Del.*, vol. 20, no. 2, pp. 710-721, Apr. 2005.

[6] M. Majidi, M. Etezadi-Amoli, and M. S. Fadali, “A novel method for single and simultaneous fault location in distribution networks,” *IEEE Trans. Power Syst.*, vol. 30, no. 6, pp. 3368-3376, Nov. 2015.

[7] R. H. Salim, M. Resener, A. D. Filomena, K. R. Caino de Oliveira, and A. S. Bretas, “Extended fault-location formulation for power distribution systems,” *IEEE Trans. Power Del.*, vol. 24, no. 2, pp. 508-516, Apr. 2009.

[8] R. Krishnathevar and E. E. Ngu, “Generalized impedance-based fault location for distribution systems,” *IEEE Trans. Power Del.*, vol. 27, no. 1, pp. 449-451, Jan. 2012.

[9] T. K. Roy, M. A. Mahmud, M. A. Barik, A. B. M. Nasiruzzaman, and A. M. T. Oo, “A nonlinear backstepping control scheme for rapid earth fault current limiters in resonant grounded power distribution systems: applications for mitigating powerline bushfires,” *IEEE J. Emerg. Select. Topics Ind. Electron.*, vol. 3, no. 2, pp. 362-371, Apr. 2022.

[10] Three-phase PI section line, MATLAB Simulink, MathWorks. Available on: (https://www.mathworks.com/help/physmod/sps/powersys/ref/threephasepisectionline.html)

[11] T. Marxsen, Powerline bushfire safety program, REFCL technologies test program-final report, December 2015. Available on: (https://www.energy.vic.gov.au/).

[12] T. K. Roy, M. A. Mahmud, A. B. M. Nasiruzzaman, M. A. Barik, and A. M. T. Oo, “A non-singular fast terminal sliding mode control scheme for residual current compensation inverters in compensated distribution networks to mitigate powerline bushfires,” *IET Generation, Transmission and Distribution*, 15, 1421–1434 (2021). https://doi.org/10.1049/gtd2.12110.

[13] T. K. Roy and M. A. Mahmud, “Fault current compensations in resonant grounded distribution systems to mitigate powerline bushfires using a nonsingular terminal sliding model controller*,” IET Generation, Transmission and Distribution*, 16, 479–491 (2022). https://doi.org/10.1049/gtd2.12294.

[14] T. K. Roy, M. A. Mahmud, S. K. Ghosh, M. A. H. Pramanik, R. Kumar and A. M. T. Oo, “Design of an Adaptive Sliding Mode Controller for Rapid Earth Fault Current Limiters in Resonant Grounded Distribution Networks to Mitigate Powerline Bushfires,” 2021 *IEEE Texas Power and Energy Conference* (TPEC), 2021, pp. 1-6, doi: 10.1109/TPEC51183.2021.9384989.

[15] J. J. Grainger and W. D. Stevenson, "Power System Analysis," McGraw-Hill, 1994.

[16] H. Saadat, “Power System Analysis,” McGraw-Hill, 2002.